HHS Public Access

Author manuscript

Clin Neurophysiol. Author manuscript; available in PMC 2017 January 01.

Published in final edited form as:

Clin Neurophysiol. 2016 January ; 127(1): 254–269. doi:10.1016/j.clinph.2015.03.004.

Spectral and source structural development of mu and alpha rhythms from infancy through adulthood

Samuel G. Thorpe[*], **Erin N. Cannon**, and **Nathan A. Fox**

University of Maryland Child Development Laboratory, 3304 Benjamin Building, College Park, MD, USA

Erin N. Cannon: ecannon@umd.edu; Nathan A. Fox: fox@umd.edu

Abstract

Objective—To assess the developmental trajectory of spectral, topographic, and source structural properties of functional mu desynchronization (characterized during voluntary reaching/grasping movement), and investigate its spectral/topographic relation to spontaneous EEG in the developing alpha band.

Methods—Event related desynchronization (ERD) and power spectral density spectra/topography are analyzed in twelve month-old infants, four year-old children, and adults. Age-matched head models derived from structural MRI are used to obtain current density reconstructions of mu desynchronization across the cortical surface.

Results—Infant/child EEG contains spectral peaks evident in both the upper and lower developing alpha band, and spectral/topographic properties of functionally identified mu rhythm strongly reflect those of upper alpha in all subject groups. Source reconstructions show distributed frontoparietal patterns of cortical mu desynchronization concentrated in specific central and parietal regions which are consistent across age groups.

Conclusions—Peak frequencies of mu desynchronization and spontaneous alpha band EEG increase with age, and characteristic mu topography/source-structure is evident in development at least as early as twelve months.

Significance—Results provide evidence for a cortically distributed functional mu network, with spontaneous activity measurable in the upper alpha band throughout development.

Keywords

EEG; mu rhythm; motor development

[*]Corresponding Author: Samuel G. Thorpe, University of Maryland Child Development Laboratory, 3304 Benjamin Building, College Park, MD, USA 20742-1131, Tel.: +1-951-255-5325, sthorpe1@umd.edu.

Conflict of Interest

None of the authors have potential conflicts of interest to be disclosed.

1. Introduction

Mu-rhythm has received renewed attention from cognitive neuroscientists in the past decade, owing in part to its proposed association with a putative human mirror neuron system (Pineda 2005, Marshall et al. 2011a). As such it has grown increasingly important to characterize the properties of this signal in greater detail, thereby allowing researchers to assess cognitive and behavioral associations with mu rhythm independent from the other rhythms present at overlapping frequencies in human EEG (Basar et al. 1999; Nunez et al. 2001). This is especially important in developmental studies, since the properties of mu rhythm are less well established for infants/children than for adults. However, numerous studies have provided strong evidence for an infant/child analogue of adult mu (Smith 1939; Smith 1941; Hagne et al. 1973; Stroganova et al. 1999; Marshall et al. 2002), referred to as infant/child central rhythm. Such studies have used the established properties of adult mu rhythm as a guide for their investigations, and gauge for comparison. In this work, we compare these properties across adult and infant/child populations directly to more clearly elucidate their development.

1.1 Adult Mu Rhythm

In the decades since its early descriptions, adult mu rhythm has been characterized by a suite of three defining properties: topographic specificity, spectral specificity, and functional dependence on behavior. Functionally, mu rhythm has long been known to desynchronize in response to voluntary motor movement (Gaustaut and Dongier 1954; Chatrian et al. 1959). Unlike posterior alpha, it is not strongly affected by changes in ambient light (Kuhlman 1978). A large body of work has since established that mu rhythm also desynchronizes in response to somatosensory stimulation (Pfurtscheller 1989; Salenius et al. 1997), imagined movements (Wolpaw et al. 2004; Pfurtscheller et al. 2006), observed movement (Gaustaut and Bert 1954; Pineda et al. 2000; Muthukumaraswamy et al. 2004), and shifting spatial attention (Covello et al. 1975; Jones et al. 2010; Bauer et al. 2012, Thorpe et al. 2012). Though modulation of alpha rhythm by spatial attention has been well studied for many years (Foxe et al. 1998; Worden et al. 2000), the comparatively recent work examining its effects on mu has shown that modulation of both rhythms can occur simultaneously in anticipation of attended stimuli across multiple modalities, including vision and somatosensation (Bauer et al. 2012), as well as audition (Thorpe et al. 2012). Still, studies comparing desynchronization across conditions (such as execute versus observed or imagined movements) have shown it to be most robust in response to motor execution (Pineda et al. 2000; Muthukumaraswamy et al. 2004). As such, motor execution has become the gold standard for functional definitions of mu rhythm.

Adult mu rhythm peaks in the same 8 – 13 Hz frequency band as posterior alpha rhythm. This spectral overlap complicates the task of distinguishing between mu and alpha rhythms, especially since it has been shown the two rhythms cohabit overlapping cortical areas (including central regions) to some degree (Andrew et al. 1997). Nonetheless, the two rhythms remain functionally distinct, and possess differentiable topographic/source distributions (Manshandren et al. 2002). Recent studies have provided evidence for a division between upper (10 – 13 Hz) and lower (8 – 10 Hz) mu band rhythms (Pfurtscheller

2000). Pfurtscheller et al. (2000) argue for different functional and topographic properties within these bands, with the upper band showing a more topographically focused, movement-type specific ERD pattern, in contrast to a more widespread and generalized pattern in the lower band. In addition, several studies provide evidence for a beta band (15 – 25 Hz) component to adult mu-rhythm (Salmelin and Hari 1994; Hari et al. 1997; Ritter 2009). These studies argue for a topographic distinction between the high and low bands, with the high frequency beta component possessing a more anterior (pre-central) spatial distribution compared to the traditional 8 – 13 Hz activity, which they argue has a post-central locus.

Mu rhythm is typically described as attaining maximal amplitude at central scalp regions. This specificity extends to studies of event related desynchronization (ERD) which have shown that mu rhythm reliably desynchronizes over these regions (Pfurtscheller 1979; Pfurtscheller 1989), and that central desynchronization is greater than that observed over other areas of the scalp (Frenkel-Toledo et al. 2013). Studies which have attempted source reconstructions of mu activity via equivalent current dipole (ECD) models have concluded various frequency components of the rhythm localize primarily to motor and somatosensory cortices (Salmelin et al. 1994a; Salmelin 1994b; Salmelin et al. 1995; Hari et al. 1997), although Salmelin and colleagues (1995) did show evidence for reactive posterior parietal sources of 10 Hz mu activity which were suppressed by finger and toe movement. However, questions remain concerning the extent of the source distribution underlying mu activity stemming from methodological considerations of these early studies. First, it is known that MEG is maximally sensitive to activity of sources located tangentially with respect to the scalp (Nunez and Srinivasan 2006). The tight clustering of mu sources about the central sulcus observed in MEG studies may be due to relative insensitivity to radially oriented sources located along various cortical gyri which are more readily detected using EEG. Indeed, an additional study using ECD modeling with simultaneously recorded EEG and MEG showed that, while MEG sources did cluster about the central sulcus, EEG sources were more widely distributed throughout central and parietal areas (Manshanden et al. 2002). Second, dipolar fits of oscillatory MEG activity in these studies only occasionally exceed the authors' goodness of fit threshold (typically greater than 90% of measured field variance). Hari et al. (1997) explain that, in their experience, dipolar fits are only adequate for 1 – 3% of evaluated time points, suggesting that most of the time more complicated source distributions are required to explain the variability in scalp recorded mu rhythm.

Adding to these concerns, much evidence exists which suggests that mu rhythm is not exclusively constrained to central scalp locations. Indeed, numerous EEG studies also report desynchronization of mu band activity over parietal and frontal electrodes in response to motor execution (Cochin et al 1999; Frenkel-Toledo et al. 2013). There has also been disagreement in electrocorticographic (EcoG) studies of mu desynchronization, with some authors reporting somatotopically mapped ERD specific to sensorimotor cortices (Arroyo et al. 1993), while others have argued that diffuse bilateral responses observed for voluntary unilateral limb movements evidence a more distributed underlying cortical network (Crone et al. 1998). Such reports corroborate neuroimaging studies which show parietal cortex, in particular, to be active in tasks involving motor planning and execution (Buneo et al. 2002; Connoly et al. 2003); motor imagery (Hanakawa et al. 2003; Solodkin et al. 2004), motor

observation (Van Overwalle and Baetens 2009; Molenberghs al. 2012), as well as saccade production and shifting spatial attention (Corbetta et al. 1998; Gitelman et al. 1999). Indeed, parietal cortex is known to subserve precisely the type of visuomotor integration required for the reaching/grasping tasks often employed in EEG studies of mu rhythm (Culham and Valyear 2006; Iacoboni 2006). Mu suppression has even been shown to correlate with fluctuations of BOLD signal in premotor and parietal areas (Arnstein et al. 2011). Such evidence suggests that mu rhythm more likely reflects synchronous activity in a an extended fronto-parietal network supporting the coordination and execution of complex motor plans, thereby obviating the need for evaluation of mu source activity across the entire cortical surface.

1.2 Infant/Child Central Rhythm

Early studies of infant EEG established that the dominant frequencies observable on the infant scalp are much lower than those observed for adults (Lindsley 1939; Smith 1938a; Smith 1938b). In contrast to occipital rhythms, the infant “central alpha” observed by Smith (1939; 1941) was not readily blocked by the opening of eyes. Thus, some rudimentary elements of the same topographic, spectral, and functional properties which have come to define adult mu rhythm have been evident in the infant central rhythm from the very beginning of its study. To date, numerous results concerning the functional properties of infant/child central rhythm have been reported. These studies have focused primarily on the functional dependence of alpha-band infant/child EEG on voluntary motor behavior (Southgate et al. 2009, 2010; Marshall et al. 2011b), observed motor behavior (Van Elk et al. 2008; Stapel et al. 2010; Nystrom 2011), and changes in ambient visual stimulation (Galkina and Boravova 1996; Stroganova et al. 1999). Together, these studies have established that infant/child central rhythm shows much of the same functional dependence on behavior as that observed for adult mu rhythm.

Contemporary developmental studies suggest a practical range of roughly 6 – 9 Hz is sufficient to capture developing mu dynamics over the first few years of life (Stroganova et al. 1999; Marshall et al. 2002). These studies defined the developing mu band via the presence of peaks observable in the power spectra of central electrodes which were not enhanced by decreases in ambient light (Stroganova et al. 1999), or else not clearly discernible at other scalp locations (Marshall et al. 2002). These findings are largely corroborated by Berchicci et al. (2011) who undertook a systematic MEG study tracking the development of mu rhythm defined functionally (via desynchronization during prehensile squeezing of a soft pipette) in infant, preschool, and adult populations. Although this study focused only on a cluster of sensors located over central areas of the left cerebral hemisphere, the results indicate the average frequency of peak mu desynchronization increased rapidly over the first year of life, from roughly 3 to 8 Hz, with the increase slowing considerably between the ages of 2 – 4 years, and eventually stabilizing near 10 Hz in adulthood.

Far less is known concerning the topographic distribution of mu throughout development than has been determined for adults, although at least one study comparing desynchronization across the scalp in response to motor execution has shown statistical

significance restricted to central electrodes (Marshall et al. 2011b). Topographic structure remains among the open questions in developmental mu research, as the distribution of neural populations (and resultant scalp locations) which exhibit desynchronization during the planning and execution of a given motor act could conceivably vary throughout development. In their illuminating review, Marshall et al. (2011a) stressed the importance of comparison across electrodes covering multiple areas of the scalp, with the aim of advancing the study of topographic specificity of the rhythm. Still, most developmental studies of mu rhythm do not make a point to show topographic comparisons via visualization of mu derived metrics across a full scalp-wide array of EEG/MEG sensors. In this study we investigate scalp wide topography of mu desynchronization throughout development, as well as, uniquely, its underlying source structure.

In addition to uncertainty concerning the topographic/source-structural trajectory of mu rhythm development, a number of other questions remain. Specifically, the nature of the relationship between the spectral trajectories of developing mu and alpha rhythms is currently unknown. That is, it is currently unclear whether the spectral content of these rhythms necessarily coincide throughout development, or whether their trajectories, while possibly similar, evolve independently of one another. Berchicci et al. (2011) is the first study to track the development of functionally defined mu rhythm across multiple subject populations using the same voluntary motor execution task for each group, but its limitations include both the restriction of analyses to small clusters of central electrodes, as well as the lack of relating the spectral structure of mu desynchronization to the dominant frequencies observed spontaneously on the scalp.

In the current study we address these issues by consideration of the scalp wide structure of both mu desynchronization and spontaneous alpha rhythms together in three age groups consisting of 12-month old infants, 4-year old children, and adults. We identify the evolving spectral and topographic characteristics of mu rhythm defined functionally via desynchronization in response to execution of a reaching/grasping movement. Additionally, we show that spontaneous EEG for all subject groups contains spectral peaks in both the lower and upper developing alpha band, and we compare the relative topographies of these peaks. Finally, we investigate structural development of mu-rhythm via sLoreta source reconstructions to assess cortical desynchronization during motor execution. The data suggest the spectral and topographic development of functionally defined mu-rhythm is tightly locked to that of the upper alpha band, and that patterns of desynchronization observed on the scalp during movement involve distributed frontal and parietal cortical areas.

2. Methods

2.1 Participants

Adult subjects consisted of 20 participants (11 female, 9 male) ranging in age from 18 to 21 years (Mean = 20; SD = 0.9). 4-year subjects consisted of 47 participants (21 female, 26 male) ranging in age from 45 to 68 months (Mean = 50; SD = 6.7). 12-month subjects consisted of 50 participants (24 female, 26 male) ranging in age from 11.4 to 12.7 months (Mean = 12.2; SD = 0.37). An additional nine 4-year olds as well as three 12-month old

were tested but excluded from the analyses due to either excessive fussiness before the onset of EEG recording (n = 7 for 4-year, 1 for 12-month), or a lack of resultant artifact-free usable data (n = 2 for 4-year, 2 for 12-month).

2.2 Experimental Set-up and Procedure

Figure 1C shows the general layout of the subject, and experimental equipment. A puppet stage was set up on a table covered with black cloth in a testing room. A curtain at the front of the stage was raised/lowered at the onset/offset of each trial interval. A video camera at the back of the stage captured the subject's behavior on each trial. A PC running E-prime 2.0 software (Psychology Software Tools, Inc., Sharpsburg, PA) sent event timing information acquired via experimenter button-press (E-prime button box info) to an EEG acquisition computer running Net Station version 4.5.1 (Electrical Geodesics, Inc., Eugene, OR). Subjects were seated in a chair (or on their caregiver's lap) approximately 40 cm from the edge of the stage. Each trial consisted of a three-second baseline interval followed by a grasp execution interval during which the subject was prompted to reach towards and grasp the toy.

During the baseline period, adult and 4-year subjects viewed a white foam core board (28 × 23 cm) with a black shape or pattern (Figure 1B). For 12-month subjects these images failed to adequately capture attention during piloting, so a moving pinwheel was presented instead. An experimenter signaled the beginning of each baseline interval to E-Prime via button-press when the subject began attending the baseline stimulus, and the event marking the end of the three second interval initiated by this button press was automatically marked by E-Prime as well.

During the grasp execution interval, the toy was placed approximately 12 cm from the subject's end of the stage. As the curtain was raised, an experimenter (not visible to the subject) pushed the stage top toward the subject (via drawer casters) to within reaching distance (pictured in figure 1A). Infant subjects were given approximately 60 seconds to grasp the toy or the trial was aborted (adult and 4-year subjects typically completed the reach almost immediately after the curtain was raised). Ten unique baseline pictures and toys were presented in unique orders, randomized across subjects. Adult subjects could complete up to 20 such trials, whereas 4-year subjects could complete up to twelve, and 12-month subjects up to fifteen. Finally, interleaved with the grasp execution trials analyzed in this work were trials of an alternate "grasp observation" condition (not analyzed here) in which the subject observed an experimenter reach and grasp the toy. Additionally, 12-month subjects received a third interleaved condition in which they observed the experimenter make a communicative pointing gesture towards the toy, which was also not analyzed here.

2.3 Behavioral Coding for EEG Segmentation

Video was recorded at a resolution of 320 × 240 with a frame rate of 30 Hz, allowing accuracy of coding to within approximately 33 ms for each behavior of interest. Two independent coders viewed each video offline (100% overlap), frame-by-frame and identified the times in which the subject first touched the toy in an act that resulted in grasp completion. Inter-rater agreement, within three frames, was achieved on 90% of the trials.

Additionally, trials in which the subject appeared to make a reach, gesture, or grasping motion during the baseline period were identified and eliminated from final analysis.

2.4 EEG Data Acquisition and Pre-processing

For all subjects, EEG was recorded using an EGI Net Amps 300 high input-impedance amplifier (Electrical Geodesics, Inc., Eugene, OR). For Adult and 4-year subjects, data was acquired using a 64-channel HydroCel Geodesic Sensor Net, whereas a 128-channel HydroCel Geodesic net was used for 12-month subjects. EEG for all subject groups was sampled at 500 Hz, and impedance values for all EEG channels were below the manufacturer recommended limit of 100 k at the start of data acquisition (50 k for Adult and four year subjects). In order to deal with data/event timing offset introduced by the NA300 anti-aliasing filter (detailed in an advisory notice released by EGI in August 2014), all events marked in the continuous recording were moved back in time by the manufacturer specified offset of 18 ms. Continuous data from the entire recording session of each subject were then baseline corrected, and average referenced. By default we excluded from this reference a set of channels from each net which lie about the sides of the face and eyes, and as such are heavily prone to net displacement artifact. Specifically, these were channels 23, 55, and 61 – 64 for the 64 channel net and 38, 43, 44, 48, 49, 113, 114, 119, 120, 121, and 125 – 128 for the 128 channel net. Additionally, the data were forward/reverse Butterworth filtered (pass band 1 – 50 Hz, stop band 0.1 – 59 Hz, 3 dB ripple, 10 dB attenuation from pass to stop band).

2.5 EEG Artifact Rejection

Continuous data were artifact edited using a thresholding procedure to remove high amplitude waveforms associated with egregious movement artifact. The procedure was applied as follows – First, the continuous data was broken into adjacent 250 ms epochs. Epochs for which more than 5 channels exceeded a threshold of +/−150 microvolts were deemed bad, and removed from the record (the sample numbers of all such discontinuities were recorded for purposes of later segmentation). For each epoch removed from the record, the previous and subsequent epochs were smoothed to zero for each channel by an inverted Hanning window of 500 ms centered on the discontinuity. Individual channels which exceeded threshold on more than 10 percent of epochs were deemed bad, and their data was interpolated (spherical spline with age-matched electrode coordinates described section 2.9) from the set of good channels for all epochs. This resulted in an additional average 0.3 (SD = 0.73), 0.34 (SD = 0.67), and 2.51 (SD = 1.42) channels being interpolated per subject for adult, 4-year, and 12-month subjects, respectively. Additionally, data for good channels which exceeded threshold in individual epochs not meeting the requirement to be dropped were interpolated within said epoch from the set of good sub-threshold channels.

The resulting data were then decomposed into Independent Components using the fastica algorithm developed by Aapo Hyvärinen and colleagues (1999, 2004), implemented in Matlab (R2013a; Natick, MA). Components related to eye movement and net displacement over the front of the head were identified for rejection using a two-fold criterion. First, rejected components had to have greatest loading magnitude at one of a designated set of channels located over the most anterior part of the head (closest to the eyes). Specifically,

these were channels 1, 5, 10, 17, 18 and 58 for the 64 channel net, and channels 1, 2, 8, 9, 14, 15, 21, 22, 25, 26, 32, and 122 for the 128 channel net. Second, rejected components had to have peak spectral power outside a band of interest decided on as 4 – 16 Hz. This second criterion ensured we only rejected frontally dominate components with EEG peaked in either the 0 – 4 Hz delta band (such as the components related to blink/saccade waveforms) or >16 Hz (such as components related to high frequency broadband muscle artifact). This procedure resulted in an average of 8.15 (SD = 1.76) ICA components being rejected for Adult subjects, 7.85 (SD = 1.72) for 4-year subjects, and 14.43 (SD = 2.9) for 12-month subjects. Artifact cleaned data were then reconstructed in channel space from the remaining set of good components, resulting in a single (discontinuous) recording of average length 19.74 (SD = 1.85), 20.96 (SD = 5.3), and 19.79 (SD = 6.56) minutes for 12-month, 4-Year, and adult subjects, respectively.

2.6 Alpha Spectral Peak Analysis and Bootstrapping

To assess the presence of spectral peaks in the alpha range we obtained power spectral density (PSD) estimates via Welch's method (pwelch.m) from the complete set of artifact edited data for each subject. Using the full set of artifact edited data both maximizes the amount of data available for analysis, as well as ensures the contribution from any particular cognitive/behavioral event occurring during the recording is made relatively minor. The data can be considered spontaneous in the sense that its spectral characteristics are reflective of a subject's aggregate cognitive/behavioral functioning over an extended period of time. We specified a DFT window length of 5 seconds at 50% overlap, which determined a frequency resolution of 0.2 Hz. For each subject, the resultant PSD were then log transformed: log PSD = $\log_{10}(1 + \text{PSD})$. This transform has the dual benefits of increasing normality while preserving the functional range of zero to infinity for log PSD values.

To assess the variability in the expected log PSD in each age group we computed empirical bootstrap distributions at each channel and frequency. Each bootstrap sample was computed as follows: First, log PSD distributions were sampled (with replacement) from all subjects a total of N_s times, where N_s is the number of subjects in each group (Efron and Tibshirani, 1994). Log PSD were then averaged across these samples to obtain a single estimate of the mean log PSD for each channel/frequency. This process was repeated 10,000 times, resulting in distributions describing the variability in expected log PSD for each channel/frequency pair.

To determine alpha frequency bands of interest for each age group we averaged each bootstrap sample across channels, then defined an "alpha spectral peak" as any frequency in a broadly defined band of interest (set as 4 – 13 Hz for all age groups) which showed greater averaged log PSD than both its adjacent neighbors. For each bootstrap sample we recorded any frequency which met these criterion, resulting in a single empirical distribution describing the variability in peak alpha frequencies for each subject group. From these empirical distributions we identified upper and lower alpha frequency bands of interest containing greater than 98.75% of all identified peaks for each age group. For 4-year and 12-month subjects, peak distributions showed distinct clusters in lower/upper bands, whereas adult subjects showed a single broad cluster of peaks spanning both bands (see section 3.1).

To assess the significance of differences between the mean frequencies of these clusters across age groups, empirical p-values were computed (see Efron and Tibshirani 1993; chapter 13) by finding the percentage of all pair-wise comparisons between frequencies in each cluster for which the difference was less than zero, such that (by convention) small empirical p-values indicate significantly higher cluster means for the older of the two age groups compared. Empirical p-values were then Bonferroni corrected (multiplied by three) to account for comparisons across multiple subject groups (Adult vs 4-year subjects, Adult vs 12-month subjects, and 4-year vs 12-month subjects).

We compared frontal to occipital alpha band PSD across age groups by first averaging bootstrap samples for each channel across all identified alpha band frequencies (combined upper/lower bands), then averaging over frontal and occipital channel groups of interest identified from the scalp topography. Bootstrap distributions describing relative amount of frontal to occipital power were then computed for each subject group as ten times the log ratio of frontal to occipital PSD. To assess significance between distributions across age groups, empirical p-values were computed by finding the percentage of all pair-wise comparisons for which the difference between subject groups was less than zero, such that (by convention) small empirical p-values indicate significantly greater frontal PSD (relative to occipital) for the older of the two age groups compared. Empirical p-values were then Bonferroni corrected to account for multiple comparisons.

To assess topographic differences between the upper and lower alpha bands within each subject group, we computed the ratio of normalized log PSD in the upper and lower bands for each channel. To do so, we first summed log PSD across each frequency in the respective bands, and then normalized this total by the sum across all channels. The normalization allowed comparison of each channel's contribution to the band-averaged PSD even though the two bands had differing amounts of total power density. We then compared upper to lower band estimates via log ratio in dB units. To assess significance of these differences, we computed this same measure for each of the 10,000 log PSD bootstrap samples described above, resulting in a distribution of topographic difference scores for each channel. Empirical p-values were computed by finding the percentage of samples for which the ratio of normalized power in the upper to lower alpha bands was less than zero, so that channels with very small empirical p-values showed greater contribution to upper alpha band topography relative to lower alpha. To control for family wise error rate (FWE) we employed Holm's (1979) sequentially rejective step-down algorithm for p-value correction (Westfall and Young 1993). Channels with corrected p-values less than a critical value of 0.05 were deemed significant.

2.7 EEG Segmentation for ERD analysis

For ERD analysis, data were segmented into individual trials, each containing a baseline and corresponding grasp execution interval. The grasp execution interval for each trial was taken as the two second interval centered on the event marking the completion of the grasp (i.e. ranging one second prior to one second post grasp). For all subject groups, the corresponding baseline interval for each trial was taken as the two second interval beginning one half second after the onset of the baseline event, during which the subject was attending

the static baseline image (adults and 4-year subjects), or pinwheel (12-month subjects). Importantly, for all subject groups any trials for which the earlier artifact thresholding procedure resulted in a discontinuity occurring anywhere in the window of analysis for either the baseline or grasp execution interval were subsequently excluded from further analysis. In total, these procedures resulted in a final pool of 394 trials for Adult subjects (mean = 19.7 per subject, SD = 0.67), 494 trials for 4-year subjects (mean = 10.5 per subject, SD = 2.23), and 231 trials for 12-month subjects (mean = 4.7 per subject, SD = 2.63).

2.8 Mu Spectral Peak Analysis and Bootstrapping

For each subject, Fourier coefficients for segmented baseline and grasp execution data were obtained via discrete Fourier transform (fft.m), corresponding to frequencies ranging from 0 – 250 Hz (Nyquist) in steps of 0.5 Hz. Of these the subset corresponding to 1 – 25 Hz were analyzed. ERD scores for each frequency, channel, and trial were then computed as ten times the log ratio of grasp execution to baseline power, i.e. decibel (dB) difference. Thus large negative ERD scores reflect strong desynchronization with respect to baseline.

To determine the frequencies for each age group which showed strong statistical evidence for desynchronization we computed empirical bootstrap distributions for ERD at each frequency by pooling all trials across subjects in each group. Each bootstrap sample was computed as follows: First, ERD distributions were sampled from all trials (with replacement) a total of N_t times, where N_t is the number of pooled trials for each group. ERD were then averaged across these samples and then across channels to obtain a single estimate of the mean ERD across frequencies. This process was repeated 10,000 times, resulting in a distribution describing the variability in expected ERD spectra. For each frequency, empirical p-values were computed by finding the percentage of bootstrap samples for which ERD was greater than zero, so that frequencies with very small empirical p-values showed strong evidence for desynchronization. As before (section 2.6), p-values were adjusted to control for multiple comparisons by Holmes' step-down correction, and only corrected empirical p-values less than 0.05 were deemed significant.

To determine the mu frequency band of interest for each age group we computed empirical bootstrap distributions for the peak frequency of the ERD spectrum using the distribution of bootstrap samples described above. For each of these 10,000 samples, the frequency for which this estimate attained the largest *negative* value was identified, resulting in a single distribution describing the variability in frequencies which show maximal desynchronization across channels for each age group. From these empirical distributions we identified functional mu frequency bands of interest for subsequent topographic and source localization analysis which contained ERD peaks for greater than 98.8% of all bootstrap samples (see sections 2.10, and 3.3, 3.4). To assess the significance of differences between the mean frequencies of ERD peak distributions across age groups, empirical p-values were computed by finding the percentage of all pair-wise comparisons between frequencies in each distribution for which the difference was less than zero, such that (by convention) small empirical p-values indicate significantly higher mean peak ERD frequency for the older of

the two age groups compared. Empirical p-values were then Bonferroni corrected to account for comparisons across multiple subject groups.

2.9 Head Model Generation

Age-matched head models for adults and twelve month olds were constructed using averaged T1-weighted anatomical MRI (three Tesla MPRAGE) from the University of South Carolina McCausland Brain Imaging Center (MCBI) Neurodevelopmental MRI Database (http://jerlab.psych.sc.edu/NeurodevelopmentalMRIDatabase, for further details see Sanchez et al. 2012a; Sanchez et al. 2012b; Richards JE 2009; Richards JE 2010). The adult template was derived from a pool of 108 adult participants aged 20 – 24 years (see Sanchez et al. 2012). The 12-month template was similarly derived (see Sanchez et al. 2011) from 10 participants aged 365 – 383 days. The four year head model was constructed using a 1.5 Tesla template from the NIH Pediatric MRI Database (NIHPD; Almi et al. 2007; Evans et al. 2006), which was derived from 19 participants aged 47 – 53 months.

Also provided for each age group were average fiducial landmark coordinates (Vertex, Naision, Inion, Left/Right Pre-auricular, and Left/Right Mastoid) coregistered with average scalp electrode coordinates for the EGI 128-channel HydroCel Sensor Net. The adult electrode positions were collected from a pool of 38 participants (for whom structural MRI was also obtained) using EGI's Geodesic Photogrammetry System (GPS). Individual MRI from each participant were registered to the average adult MRI template, and electrodes positions were transformed to the adult head and averaged across subjects. The 12-month coordinates came from a pool of 10 participants also using EGI GPS, who also underwent individual structural MRI. Positions of the seven fiducial electrodes were recorded for each participant, and used to map the adult electrode positions to the infant, which were then averaged across subjects. Finally, the 4-year electrode positions were derived via registration of the Adult MRI template to the 4 year template, then linearly transforming the adult electrodes to the 4 year old space.

Electrode coordinates were coregistered with the head models using Matlab's built in fminseach.m to find the set of xyz-scalings, and roll, pitch, and yaw rotations which minimize the sum square distance between the provided fiducial landmarks and those visually identified on the scalp of the head model. This same transformation was then applied to the set of averaged electrode coordinates. Lastly, the resultant transformed coordinates were set to their nearest (euclidean) neighbors on the scalp mesh (see below). Since the EGI 64 channel HydroCel net is designed to cover a proper subset of the scalp locations covered by the 128 channel HydroCel net, we used for the Adult and 4-year subject populations the coordinates (in 128 channel space) of the 64 channel subset to which 64 channel net electrodes map.

Cortical surface meshes and parcellation atlases (Desikan at al. 2006) for each age group were extracted from the age-matched T1-weighted templates using FreeSurfer v5.3 (documented and freely available online at http://surfer.nmr.mgh.harvard.edu/). To reduce computational load associated with lead field computation, the cortical surface mesh was downsampled to 36,000 nodes using iso2mesh software (Fang et al, 2009). Boundary Element Method (BEM) forward models were constructed for each age group (see Figure 2)

consisting of four homogeneous compartments corresponding to scalp, skull, intracranial space, and gray matter. Meshes for these surfaces were extracted from the MRI templates using MNE software (Gramfort et al. 2014), and forward models were computed using openMEEG (Gramfort et al. 2010; Kybic et al. 2005) with commonly used conductivity values of 0.33, 1.67, 0.0042, and 0.33 for gray matter, intracranial space, skull, and scalp, respectively.

2.10 Mu Desynchronization Cortical Localization and Bootstrapping

To determine which areas of the brain showed greatest desynchronization in the previously identified mu-frequency band we did separate current density reconstructions for baseline and grasp execution intervals for each frequency in the identified band using the sLoreta inverse - a minimum energy solution standardized by an estimate of variance in the forward model for each cortical node (Pascual-Marqui 2002). The regularization parameter (α) was chosen to minimize cross-validation error (see Pascual-Marqui 1999; Stone 1974 for details) averaged across mu-band frequencies. A single value for α was found for all subject groups by computing cross-validation error over a range of α-values (1e-9, 1e-8, 1e-7, 1e-6, 1e-5, 1e-4, 1e-3, 1e-2, 1e-1) for both baseline and grasp execution intervals for each mu-band frequency on every trial, and subsequently averaging these estimates across intervals/frequencies/trials to obtain a single cross-validation error estimate for each choice of α. The α-value associated with the smallest mean cross-validation error for each subject group was α = 1e-4, which matches the value used in many previous studies using Loreta solutions with EEG (Congedo et al. 2006; Lamm et al. 2012).

Analogous to the computation for scalp electrodes, ERD was computed on the cortical surface mesh for each mu-band frequency on each trial as ten times the log ratio of grasp execution to baseline current density. These were then averaged across frequencies to provide a single estimate of mu-band ERD for each cortical node on each trial. To test for significance, we bootstrapped empirical mu-band ERD distributions for each cortical node. Each bootstrap sample was computed by sampling (with replacement) from the full set of trials pooled across subjects in each group, and averaging mu-band ERD across the sample. This process was repeated 10,000 times, resulting in empirical distributions describing the variability in expected mu-band ERD at each cortical node. Empirical p-values were computed for each node by finding the percentage of samples for which mu-band ERD was greater than zero, so that nodes with very small empirical p-values showed significant ERD. As before (sections 2.6, 2.8), empirical p-values were corrected via Holm's sequentially rejective step-down algorithm, and nodes with corrected p-values less than a critical value of 0.05 were deemed significant.

3 Results

3.1 Alpha Band Power Spectral Density

Figure 3A, C, E (left column) shows log power spectral density by frequency for each subject group. Average log PSD across subjects is indicated by the red bars, whereas transparent light red bars indicate the 95th percentile of log PSD values obtained via bootstrap sampling. The peak histograms in figure 3B, D, F (right column) depict the

variability across bootstrap samples in frequencies at which alpha spectral peaks (between 4 – 13 Hz) were found. For the 12-month subject group (3A), a pair of peaks in the log PSD spectrum is evident. From the peak histogram in 3B it can be seen that the frequencies at which PSD peaks occurred across samples were concentrated in two distinct clusters corresponding to the peaks in the mean spectrum. These clusters had mean frequencies of 4.49 and 7.39 Hz, respectively. For 4-year subjects a similar pair of peaks are evident in the log PSD spectrum at slightly higher frequencies (3C), and the peak histogram for this group (3D) also shows two distinct clusters corresponding to the peaks in the mean spectrum. The mean frequencies for the clusters in this age group were 6.61 and 8.81 Hz, respectively. Bootstrap comparisons showed that the mean frequencies of alpha peaks in the lower and upper band clusters was significantly higher for 4-year than for 12-month subjects (Bonferroni corrected empirical $p \ll 0.01$, as described in section 2.6).

For both 12-month and 4-year subjects, greater than 98.75% of all alpha peaks fell into one of two adjacent group-specific bands of 2 Hz in width, corresponding to the clusters observed in 3B, D. Specifically, 4 – 6 Hz, and 6 – 8 Hz contained the entirety of the spread in peak frequencies about the lower spectral peak for 12-month and 4-year subjects, respectively. Similarly, 6 – 8 Hz, and 8 – 10 Hz contained the frequency spread about the upper spectral peak for these subject groups. For these reasons we designated these as the lower/upper alpha bands for 12-month and 4-year subjects for further topographic analysis. For adult subjects, the log PSD spectrum (3E) did not show the same clear doubly-peaked structure as was evident for 12-month and 4-year subjects. Rather, a broad peak was evident in the mean spanning the classic adult alpha range, with a mean peak frequency of 10.51 Hz. However, like the other age groups, a single band of 4 Hz in width captured the vast majority of the spread (100% for adults) in alpha peak frequencies observed across bootstrap samples (3F). Bootstrap comparisons showed that the mean frequency of alpha peaks in this band was significantly higher than that of the upper and lower bands for 12-month subjects ($p \ll 0.01$ for both tests), as well as the lower band for 4-year subjects ($p \ll 0.01$), but not the upper band ($p = 0.1$). In line with previous studies which distinguish between upper/lower parts of the adult alpha band (Petsche et al. 1997; Pfurtscheller et al. 2000), we decided to separate this into lower (8 – 10 Hz) and upper (10 – 12 Hz) alpha bands for topographic comparison with the other subject groups.

3.2 Alpha Band Topography

Figure 4 shows upper and lower band alpha band topography (log PSD) for each subject group (left column), along with the log ratio of normalized power in the upper/lower bands masked by significance as described in section 2.6 (right column). The lower and upper alpha band topographies within each group (4A, C, E) appear qualitatively similar. Indeed, topographies for both alpha bands peak over occipital-parietal electrodes for all subject groups. One interesting difference between subject groups is that adults show a strong peak over frontal channels in both alpha bands, whereas there is no evidence of such a frontal peak for the younger subject groups (see section 4.2 for interpretations of this finding). To quantify this finding, we compared the log ratio of PSD in frontal (indicated by blue dots) and occipital (indicated by cyan) channel groups across subjects in each age group, as described in section 2.6. Our bootstrap comparisons revealed significantly greater frontal

(relative to occipital) PSD in Adults as compared to both 4-year and 12-month subjects (Bonferroni corrected empirical $p \ll 0.01$). Comparison of 4-year to 12-month subjects did not reach significance ($p > 0.05$).

The fine structure of topographic differences between bands is more readily observable when directly comparing normalized log PSD topographies via log ratio as in figure 4B, D, F. These maps are shown masked by significance (adjusted empirical $p < 0.05$ as described in 2.6) such that only data for channels which contributed significantly more to the upper alpha band (relative to lower alpha) are visualized. Here there is a similar pattern common across the scalp for all subject groups, where bilateral central electrodes show the largest relative contribution to the upper alpha band (C3/C4 electrode locations are indicated by green dots in 4B, D, E for comparison). For adults and 4-year olds (4D, F), the foci of these maps are very tightly clustered about C3/C4, whereas the distribution for 12-month olds (4B), while peaking at C3/C4, is more broadly distributed. The distinct bilateral central peaks evident in these maps have long been associated with mu rhythm topography, and as such these findings corroborate previous studies associating the upper alpha band with mu-rhythm in both adult (Andrew and Pfurtscheller 1997; Pfurtscheller et al. 2000) and infant/child subjects (Marshall et al. 2002).

3.3 ERD Spectra and Mu Band Topography

Figure 5A, C, E (left column) shows channel averaged ERD spectra from 1 – 25 Hz plotted for each age group. Average ERD across all trials is indicated by blue bars where ERD met significance for criterion, and gray bars otherwise. Black error bars indicate 95th percentile confidence intervals obtained via bootstrap sampling. Associated peak histograms in 3A, CE depict the variability across bootstrap samples in frequencies at which ERD peaks (between 1 – 25 Hz) were found. For 12 month subjects (5A) ERD shows with a clear (minimum) peak evident between 7 – 8 Hz. The associated histogram for this group shows that the frequencies at which ERD peaks occurred across bootstrap samples were strongly concentrated in this band (greater than 98.8% of observed peaks fell between 7 and 8 Hz), with a mean peak frequency of 7.5 Hz. Similar histograms for 4-year subjects (5C) show that *all* frequencies at which ERD peaked across bootstrap samples were contained in the band from 8.5 – 10 Hz, with a mean peak frequency of 9.34 Hz. Finally, for adult subjects (5E) ERD histograms show that *all* frequencies at which ERD peaked across bootstrap samples were contained in the band from 10 – 12 Hz, with a mean peak frequency of 11.29 Hz. Interestingly, this subject group alone shows strong evidence for ERD at higher frequencies as well, as nearly all frequencies from 15 – 25 Hz met significance. Such beta band desynchronization is commonly reported in adults (Salmelin and Hari 1994; Hari et al. 1997). The current results suggest this is a spectral feature of functionally defined mu-rhythm which develops after the age of four.

Across age groups, a clear pattern is evident. For 4-year and adult subjects 100% of all frequencies at which ERD peaked across bootstrap samples were contained in a single band (8.5 – 10 Hz for 4-year, 10 – 12 Hz for Adults). For 12-month subjects the peak ERD frequencies were slightly more distributed, but still greater than 98.8% of all ERD peaks across bootstrap samples were contained in the band from 7 – 8 Hz. Bootstrap comparisons

(described in section 2.8) showed that the mean frequency of peak ERD was significantly higher for adults than for 4-year and 12-month subjects (Bonferroni corrected empirical $p \ll 0.01$ for both tests), as well as higher for 4-year subjects as compared to 12-month olds (Bonferroni corrected empirical $p \ll 0.01$). For all three subject groups, the bands containing the overwhelming majority of peak ERD frequencies across bootstrap samples fell within the upper alpha bands identified spontaneously on the scalp (section 3.1). As such, we designated these as functional mu bands of interest for further topographic and cortical localization analyses.

Mu band ERD topography is depicted for each age group in figure 5 B, D, F. Again, a very similar pattern is seen across the scalp for all subject groups, where scalp maps show distinct bilateral peaks over central and anterior parietal areas (C3/C4 electrode locations are indicated by green dots for comparison). While the similarity between these maps and those from figure 4B, D, F are obvious, there is one noticeable difference which is consistent across age groups. Specifically, the bilateral peaks in the ERD maps are located over slightly more posterior scalp regions (see section 4.2 for discussion). Still, the similarity of the general pattern in sharing focal bilateral peaks at overlapping central/parietal electrodes suggest the possibility that similar neural generators underly their manifestation on the scalp.

3.4 Mu Desynchronization Cortical Localization

Figures 6, 7, and 8 depict cortical mu band desynchronization computed from sLoreta source reconstructions for adult, 4-year, and 12-month subjects respectively. Figures 6A, 7A, and 8A (top row) show the mu band ERD on the reconstructed cortical surface, whereas 6B, 7B, and 8B (middle row) display the same on the inflated surface to better visualize ERD in the cortical sulci (see Dale and Sereno 1993 for details of the method used for inflation). In both sets of maps, cortical ERD is shown masked by significance (described in section 2.10) such that only data for cortical nodes with ERD significantly less than zero (adjusted empirical p, described in section 2.10) is visualized. To summarize the cortical regions that showed the strongest desynchcronization, figures 6C, 7C, and 8C show ERD summed across all significant nodes within the top ten cortical regions for each cerebral hemisphere (defined via the Desikan 2006 cortical atlas, and ranked by summed ERD). Shown along with these rankings are representations of these areas on the cortical surface color coded by their respective rankings (brighter areas show more ERD).

Although in general mu band ERD shows a broad fronto-parietal distribution across the cortical surface, it is consistently greatest in specific central and parietal regions, which account for the majority of the top ranked cortical areas in both hemispheres. Specifically, post-central, pre-central, para-central, and superior frontal regions fall in the top ten for both hemispheres of all subject groups. Similarly, the superior parietal, and supramarginal cortices, as well as the precuneus (all parietal regions) fall into the top ten ranked areas for both hemispheres of all subject groups. Of note, inferior parietal cortex fall into the top ten regions in both hemispheres for adult and four year subjects, but ranks 12 in both hemispheres for 12-month subjects.

4 Discussion

The results of this study describe the development of functional mu rhythm together with that of spontaneous alpha-band EEG rhythms identifiable on the scalp, bearing specifically on the spectral and topographic characteristics of these rhythms. We replicate previous findings that demonstrate motor execution related mu suppression in infants showing developmental increases in peak mu frequency with age (Berchicci et al. 2011). We extend these results in revealing both the topographic pattern of mu desynchronization across the scalp, as well as source structure on the cortical surface. Additionally, we replicate previous work concerning the development of spontaneous alpha band EEG across the scalp (Marshall et al. 2002), and extend this work via identification of fine spectral and topographic structure within the alpha band related directly to functional mu-rhythm.

4.1 Spectral development of alpha and functional mu rhythm

The developmental trajectory of the peak frequency we observed for functional mu rhythm is similar to the trajectory reported by Berchicci and colleagues (2011). Whereas those authors reported a mean peak frequency of 8.25 Hz by 47 weeks (the oldest infants in their sample), we observed a slightly lower mean frequency of 7.5 Hz for the 12-month sample. This small discrepancy could be due to either (or both) our increased sample size, or the fact that we chose to incorporate ERD from the full scalp wide array of electrodes into the estimate. By age four, these authors report peak mu frequencies between 8 – 10 Hz, which is precisely in line with the current estimates. Interestingly, the current data showed that the increase in the peak mu frequency over the first years of life strongly resembles the trajectory of an upper alpha band peak observed in the spontaneous EEG. Previous developmental EEG studies with infants and children identified similar 6 – 9 Hz rhythms over central electrodes that were argued to be an infant/child analogue of adult mu (Marshall et al. 2002; Stroganova et al 1999). In showing that the spectral and topographic characteristics of this rhythm match that of functionally defined mu over the first years of life, the current data strongly support this position.

The current results further show that adult mu desynchronization peaks between 10 – 12 Hz, corroborating studies which show this upper alpha band to be of special relevance to mu (Andrew and Pfurtscheller 1997; Pfurtscheller et al. 2000). This general developmental increase in peak mu frequency with age is similar to that seen in developing alpha, which the current data also confirm continues into adulthood. A number of neurophysiological processes occurring throughout development might contribute to this process. Developmental changes in GABAergic expression and cellular dynamics unfold in rodent (Khazipov et al. 2004; Doischer et al. 2008) and primate (Hashimoto et al. 2009) brains, which have been postulated to underlie the emergence of “continuous” oscillations in pre-term human infant EEG (Vanhatalo and Kaila 2006), as well as the emergence of synchronous gamma band oscillations in childhood and their shift towards higher frequencies in adolescence (Uhlhaas et al. 2010). Work by Muthukumaraswamy et al. (2009) has shown that increased resting GABA concentration in adult occipital cortex correlates positively with the peak frequency of visually evoked gamma oscillations observed with MEG. Of particular relevance to the work here, an MEG study by Jensen et al. (2005),

showed the ~20 Hz beta component of adult mu rhythm to be modulated by administration of the GABAergic agonist benzodiazepine, though the results of this study showed the opposite relation to that observed for the gamma band, reporting *decreased* frequency with increased GABA mediated inhibition.

In general, it has been argued that the frequency of coherent oscillations between interconnected neural populations may be limited by conduction delays between them, such that coupling frequency is inversely related to delay (Kopell et al. 2000; Von Stein and Starnthein 2000). Since conduction delays between interconnected areas generally scale with the distance of spatial separation, developmental increases in relatively low-frequency EEG rhythms such as mu and alpha could result from enhanced conduction velocity along long-distance (anterior-posterior) white matter tracts via axonal growth and myelination, processes which can continue into early adulthood (Yakovlev and Lecours 1967). Interestingly, only adult subjects showed evidence for desynchronization at higher beta band frequencies. Hari and colleagues (1997) have argued this beta component to be associated with a more anterior scalp distribution relative to lower frequency mu activity. As such, the possibility that the emergence of motor related beta desynchronization in adults relates to developing interconnectivity over comparatively smaller spatial scales, possibly between sensorimotor and premotor areas, should be investigated in future work.

With regard to the spectral peak we observed for 12-month and 4-year subjects in the lower alpha band, we can only say this band does not contain the frequencies that maximally desynchronize during motor execution. However, we did find some evidence for lower alpha band desynchronization for adults and 4-year subjects in the form of significant ERD at multiple lower alpha band frequencies. Interestingly, Stoganova et al. (1999) showed evidence for a topographically distributed local peak between 4 – 5 Hz in the mean amplitude spectrum of their eight and eleven month old subjects similar to that which we observed for the twelve month olds (see figure 2 in Stronganova et al. 1999), although it is important to note that no description as such or arguments concerning this were advanced in their text. The current data suggest that the frequency of this peak also increases with age, approaching our observed value of 6.61 Hz by age four. Further, the *difference* between peak frequencies of the upper and lower alpha bands *decreased* with age, moving from 2.9 Hz at 12-months (upper/lower peaks of 7.39 and 4.49 Hz, respectively), to 2.2 Hz at four years (upper/lower peaks of 8.81 and 6.61 Hz, respectively). As we did not discern a clear doubly peaked structure in the adult spectra, one possible interpretation of these results is that the difference between peaks in these bands decreases throughout development to the point of overlapping in adulthood. If true, however, these results suggest functional differences between bands are still retained in adulthood, as evidenced by the fact that the upper alpha band contains the peak frequencies of mu desynchronization for all subject groups.

4.2 Topographic/Source structural development of alpha and functional mu rhythm

Topographic comparisons yielded a number of interesting observations. These data corroborate the long standing convention concerning the topography of mu rhythm showing bilateral focus over central electrodes, as this pattern was clearly evident for all subject groups in the desynchronization patterns we observed, as well as in the comparison of

relative power in the upper/lower alpha bands. However, we extend these results in a number of important ways. The relative power topographies we observed showed these bilateral foci peaked specifically at channels C3 and C4 (see Figure 4) where spontaneous mu rhythm is classically described as attaining maximal amplitude, whereas the pattern associated with mu desynchronization showed bilateral peaks which were slightly more posterior (Figure 5). Numerous previous studies have reported similar post-central foci of desynchronization (Hari et al. 1997, Kuhlman 1978), though the current results indicate that mu desynchronization extends to more posterior parietal areas. Such parietal desynchronization could result from the computation of visuomotor transformations required for coordinating two-dimensional retinotopically mapped visual information within a three-dimensional representation of extrapersonal space, which posterior parietal cortex specifically is thought to underlie (Bruneo et al. 2002; Iacoboni 2006).

Taken together, the current results suggest that although the network underlying functional mu rhythm seemingly extends to posterior parietal areas, the spontaneous activity of this network is most evident over the central part of the scalp. This could be due to either (or both) the cortical geometry of the functional network itself, or simply the fact that EEG waveforms recorded at parietal channels typically contain strong contributions from posterior alpha rhythm, so that spontaneous mu activity is less readily discernible. Indeed, the topographies we observed in the upper and lower alpha bands did not themselves reveal evident peaks at central electrodes. Only upon comparing the relative contribution to each band across channels did this effect become clear. Superficially, both bands showed similar topography for all subject groups, with occipital/parietal foci falling off towards more anterior scalp areas (with the exception of adult frontal peaks discussed below). One straightforward interpretation of these patterns is that activity in both bands is primarily dominated by classic posterior alpha rhythm, but that coherent oscillations within the network underlying mu rhythm are additionally embedded in the upper alpha band.

An intriguing exception to the general pattern of posterior to anterior alpha power fall off was seen for adults, who additionally showed large alpha peaks in both bands over pre-frontal electrodes. This observation is consistent with previous work showing strong frontal alpha in adult subjects (Nunez 1995; Nunez et al. 2001; Nunez and Srinivasan 2006). A developmental study conducted by Srinivasan et al. (1999) showed higher frontal alpha power in adults (relative to 6 – 11 year old children) which was associated with stronger coherence between anterior and posterior channels at alpha frequencies. Srinivasan argued these effects could be facilitated by the development of long-range corticocortical white matter fiber tracts oriented along the anterior-posterior axis, and the current data appear consistent with this interpretation as well.

The distributions of cortical desynchronization we observed were concentrated in similar frontal, central and parietal cortical regions for all subject groups. Methodologically, our study differs from previous MEG work modeling mu source activity using ECD (Salmelin et al. 1994a; Salmelin 1994b; Salmelin et al. 1995; Hari et al. 1997). As opposed to assuming a small number of dipoles underlying scalp recorded mu activity, we instead assume that cortical areas contributing to mu activity are distributed throughout the brain, then observe which areas are modulated by motor execution, thereby defining the mu network

functionally. Previous MEG studies using distributed synthetic aperture magnetometry (SAM) localizations have also analyzed functional changes in adult mu, but in these studies changes in source activity were measured in response to tactile stimulation (Gaetz and Cheyne 2003; Cheyne et al. 2006). These studies also found functional changes were primarily restricted to motor and somatosensory cortex. Our results suggest that more complicated motor actions such as voluntary reaching/grasping involving computation of the location of target objects in extrapersonal space result in a broader cortical distribution of mu desynchronization specifically including parietal areas, which may be more readily observable using EEG.

Before concluding, a couple of methodological limitations within the current study should be acknowledged. First, because we used 64 channel nets for adults and 4-year subjects as opposed to 128 channel nets for 12-month subjects, topographies and source localizations are less directly comparable than would have been the case if acquisition using the 128 channel nets for all groups would have been possible. It is for this reason that we restricted comparisons of source structure across groups to qualitative descriptions of areas which show the greatest ERD. Second, although the purpose of the baseline interval was to provide a period of quiet sustained attention, and this was seemingly achieved for all subject groups, it would be ideal for the simple visual stimuli presented during the baseline to be identical for all groups. Nonetheless, there is compelling reason to suspect we have succeeded in clarifying the picture of mu development in many respects. Specifically, the infant and 4-year ERD spectra we observed had clear peak frequencies in bands corroborating previous results which were identifiable using the same procedure which was applied to the adult data. Moreover, the infant and 4-year mu bands we identified showed topographic characteristics which were extremely similar to those observed for adults. This was not only true with respect to patterns of functional mu desynchronization, but also its spontaneous manifestation on the scalp – a measure *entirely* independent of any choice of ERD baseline. Consequently, the status of infant/child central rhythm as developmental analogue of adult mu appears increasingly unequivocal.

5 Conclusions

Mu has long been called “the second rhythm” of human EEG, where classic posterior alpha is, of course, the first (Niedermeyer 1997). Most EEG waveforms, including alpha rhythms, are believed to be generated by synchronous synaptic activity coherent over large areas of the cortical surface that are thought to extend several centimeters (Nunez 1995; Nunez and Srinivasan 2006), yet mu is still often described in the literature as a simple idling rhythm local to motor and/or somatosensory cortex. While it seems a safe premise that high amplitude mu rhythm at central electrodes is positively correlated with relative inactivity of sensorimotor areas, the topographies and source distributions we observed suggest that, at least for sufficiently complex motor actions such as reaching/grasping, mu desynchronizes in a more widely distributed pattern. The collective results are consistent with the following proposed interpretation: Mu rhythm emerges as the resonance of an interconnected frontoparietal network that supports the formulation, coordination, and execution of complex motor behavior. Synchronous activity within this network is evident on the scalp in the first year of life, in the form of spontaneous band specific EEG oscillations (particularly

discernible at central electrodes) which desynchronize during motor execution. Perhaps as a combined result of functional development within the network and simultaneous increases in the efficacy of white matter interconnectivity (e.g. tract growth and myelination), the peak frequency of network resonance increases with age. Further work relating spontaneous EEG/MEG to functional desynchronization in younger and intermediate aged subject groups could serve to expand and elaborate on this view.

Acknowledgments

We thank John E. Richards and Kayla Finch for their contributions to this work. This research was supported by NICHD PO1 HD064653.

References

Almli CR, Rivkin MJ, McKinstry RC. The NIH MRI study of normal brain development (Objective-2): newborns, infants, toddlers, and preschoolers. NeuroImage. 2007; 35:308–25. http://dx.doi.org/10.1016/j.neuroimage.2006.08.058. [PubMed: 17239623]

Andrew C, Pfurtscheller G. On the existence of different alpha band rhythms in the hand area of man. Neurosci Lett. 1997; 222:103–6. http://dx.doi.org/10.1016/S0304-3940(97)13358-4. [PubMed: 9111739]

Arnstein D, Cui F, Keysers C, Maurits NM, Gazzola V. μ-suppression during action observation and execution correlates with BOLD in dorsal premotor, inferior parietal, and SI cortices. J Neurosci. 2011; 31:14243–9.10.1523/JNEUROSCI.0963-11.2011 [PubMed: 21976509]

Arroyo S, Lesser RP, Gordon B, Uematsu S, Jackson D, Webber R. Functional significance of the mu rhythm of human cortex: an electrophysiologic study with subdural electrodes. Electroencephalogr Clin Neurophysiol. 1993; 87:76–87.10.1016/0013-4694(93)90114-B [PubMed: 7691544]

Başar E, Schürmann M, Başar-Eroglu C, Karakaş S. Alpha oscillations in brain functioning: an integrative theory. Int J Psychophysiol. 1997; 26:5–29. [PubMed: 9202992]

Bauer M, Kennett S, Driver J. Attentional selection of location and modality in vision and touch modulates low-frequency activity in associated sensory cortices. J Neurophysiol. 2012; 107:2342–51.10.1152/jn.00973.2011 [PubMed: 22323628]

Berchicci M, Zhang T, Romero L, Peters A, Annett R, Teuscher U, et al. Development of mu rhythm in infants and preschool children. Dev Neurosci. 2011; 33:130–43. http://dx.doi.org/10.1159/000329095. [PubMed: 21778699]

Buneo CA, Jarvis MR, Batista AP, Andersen RA. Direct visuomotor transformations for reaching. Nature. 2002; 416:632–6. http://dx.doi.org/10.1038/416632a. [PubMed: 11948351]

Chatrian GE, Petersen MC, Lazarte JA. The blocking of the rolandic wicket rhythm and some central changes related to movement. Electroencephalogr Clin Neurophysiol. 1959; 11:497–510. http://dx.doi.org/10.1016/0013-4694(59)90048-3. [PubMed: 13663823]

Cheyne D, Gaetz W, Garnero L, Lachaux J. Neuromagnetic imaging of cortical oscillations accompanying tactile stimulation. Brain Res Cogn Brain Res. 2003; 17:599–611. [PubMed: 14561448]

Cochin S, Barthelemy C, Roux S, Martineau J. Observation and execution of movement: similarities demonstrated by quantified electroencephalography. Eur J Neurosci. 1999; 11:1839–42.10.1046/j.1460-9568.1999.00598.x [PubMed: 10215938]

Congedo M, Lotte F, Lécuyer A. Classification of movement intention by spatially filtered electromagnetic inverse solutions. Phys Med Biol. 2006; 51:1971–89. http://dx.doi.org/10.1088/0031-9155/51/8/002. [PubMed: 16585840]

Connolly JD, Andersen RA, Goodale MA. FMRI evidence for a “parietal reach region” in the human brain. Exp Brain Res. 2003; 153:140–5. http://dx.doi.org/10.1007/s00221-003-1587-1. [PubMed: 12955383]

Corbetta M, Akbudak E, Conturo TE, Snyder AZ, Ollinger JM, Drury HA, et al. A common network of functional areas for attention and eye movements. Neuron. 1998; 21:761–73. http://dx.doi.org/10.1016/S0896-6273(00)80593-0. [PubMed: 9808463]

Covello A, de Barros-Ferreira M, Lairy GC. A telemetric study of central rhythms in children. Electroencephalogr Clin Neurophysiol. 1975; 38:307–319. http://dx.doi.org/10.1016/0013-4694(75)90252-7. [PubMed: 46809]

Crone NE, Miglioretti DL, Gordon B, Sieracki JM, Wilson MT, Uematsu S, Lesser RP. Functional mapping of human sensorimotor cortex with electrocorticographic spectral analysis I. Alpha and beta event-related desynchronization. Brain. 1998; 121:2271–99.10.1093/brain/121.12.2271 [PubMed: 9874480]

Culham JC, Valyear KF. Human parietal cortex in action. Curr Opin Neurobiol. 2006; 16:205–12. http://dx.doi.org/10.1016/j.conb.2006.03.005. [PubMed: 16563735]

Dale AM, Sereno MI. Improved Localization of Cortical Activity by Combining EEG and MEG with MRI Cortical Surface Reconstruction: A Linear Approach. J Cog Neurosci. 1993; 5:162–176. http://dx.doi.org/doi:10.1162/jocn.1993.5.2.162.

Desikan RS, Ségonne F, Fischl B, Quinn BT, Dickerson BC, Blacker D, et al. An automated labeling system for subdividing the human cerebral cortex on MRI scans into gyral based regions of interest. NeuroImage. 2006; 31:968–80. http://dx.doi.org/10.1016/j.neuroimage.2006.01.021. [PubMed: 16530430]

Doischer D, Hosp JA, Yanagawa Y, Obata K, Jonas P, Vida I, Bartos M. Postnatal differentiation of basket cells from slow to fast signaling devices. J Neurosci. 2008; 28:12956–68.10.1523/JNEUROSCI.2890-08.2008 [PubMed: 19036989]

Efron, B.; Tibshirani, RJ. Monographs on statistics and applied probability. Vol. 57. New York: Chapman and Hall; 1993. An introduction to the bootstrap.

Evans AC. The NIH MRI study of normal brain development. NeuroImage. 2006; 30:184–202. http://dx.doi.org/10.1016/j.neuroimage.2005.09.068. [PubMed: 16376577]

Fang, Q.; Boas, DA. Tetrahedral mesh generation from volumetric binary and gray-scale images. IEEE International Symposium on Biomedical Imaging: From Nano to Macro; 2009;

Foxe JJ, Simpson GV, Ahlfors SP. Parieto-occipitial ~10 Hz activity reflects anticipatory state of visual attention mechanisms. NeuroReport. 1998; 9:3929–33. [PubMed: 9875731]

Frenkel-Toledo S, Bentin S, Perry A, Liebermann DG, Soroker N. Dynamics of the EEG power in the frequency and spatial domains during observation and execution of manual movements. Brain Res. 2013; 1509:43–57. http://dx.doi.org/10.1016/j.brainres.2013.03.004. [PubMed: 23500633]

Gaetz W, Cheyne D. Localization of sensorimotor cortical rhythms induced by tactile stimulation using spatially filtered MEG. NeuroImage. 2006; 30:899–908.10.1016/j.neuroimage.2005.10.009 [PubMed: 16326116]

Galkina NS, Boravova AI. The formation of EEG mu-and alpha-rhythms in children during the second–third years of life. Hum Physiol. 1996; 22:540–5.

Gastaut HJ, Dongier MCG. On the significance of ‘wicket rhythms‘ in psychosomatic medicine. Electroencephalogr Clin Neurophysiol. 1954; 6:687. http://dx.doi.org/10.1016/0013-4694(59)90048-3.

Gastaut HJ, Bert J. EEG changes during cinematographic presentation (Moving picture activation of the EEG). Electroencephalogr Clin Neurophysiol. 1954; 6:433–44. http://dx.doi.org/10.1016/0013-4694(54)90058-9. [PubMed: 13200415]

Gramfort A, Luessi M, Larson E, Engemann D, Strohmeier D, Brodbeck C, et al. MNE software for processing MEG and EEG data. NeuroImage. 2014; 86:446–60. http://dx.doi.org/10.1016/j.neuroimage.2013.10.027. [PubMed: 24161808]

Gramfort A, Papadopoulo T, Olivi E, Clerc M. OpenMEEG: opensource software for quasistatic bioelectromagnetics. Biomed Eng Online. 2010; 9:45. http://dx.doi.org/10.1186/1475-925X-9-45. [PubMed: 20819204]

Hagne, I.; Persson, J.; Magnusson, R.; Petersen, I. Spectral analysis via fast Fourier transform of waking EEG in normal infants. In: Kellaway, P.; Petersén, I., editors. Automation of clinical electroencephalography: a conference. New York: Raven; 1973. p. 103-43.

Hanakawa T, Immisch I, Toma K, Dimyan M, Van Gelderen P, Hallett M. Functional properties of brain areas associated with motor execution and imagery. J Neurophysiol. 2003; 89:989–1002. http://dx.doi.org/10.1152/jn.00132.2002. [PubMed: 12574475]

Hari R. Activation of human primary motor cortex during action observation: A neuromagnetic study. Proc Natl Acad Sci. 1998; 95:15061–5. http://dx.doi.org/10.1073/pnas.95.25.15061. [PubMed: 9844015]

Hari R, Salmelin R, Mäkelä JP, Salenius S, Helle M. Magnetoencephalographic cortical rhythms. Int J Psychophysiol. 1997; 26:51–62. http://dx.doi.org/10.1016/S0167-8760(97)00755-1. [PubMed: 9202994]

Hashimoto T, Nguyen QL, Rotaru D, Keenan T, Arion D, Beneyto M, et al. Protracted developmental trajectories of GABAA receptor alpha1 and alpha2 subunit expression in primate prefrontal cortex. Biol Psychiatry. 2009; 65:1015–23.10.1016/j.biopsych.2009.01.004 [PubMed: 19249749]

Holm S. A simple sequentially rejective multiple test procedure. Scand J Stat. 1979; 6:65–70.

Hyvärinen A. Fast and robust fixed-point algorithms for independent component analysis. IEEE Trans Neural Netw. 1999; 10:626–34. http://dx.doi.org/10.1109/72.761722. [PubMed: 18252563]

Hyvärinen A, Hurri J. Blind separation of sources that have spatiotemporal variance dependencies. Signal Process. 2004; 84:247–254. http://dx.doi.org/10.1016/j.sigpro.2003.10.010.

Iacoboni M. Visuo-motor integration and control in the human posterior parietal cortex: evidence from TMS and fMRI. Neuropsychologia. 2006; 44:2691–9. http://dx.doi.org/10.1016/j.neuropsychologia.2006.04.029. [PubMed: 16759673]

Jensen O, Goel P, Kopell N, Pohja M, Hari R, Ermentrout B. On the human sensorimotor-cortex beta rhythm: sources and modeling. NeuroImage. 2005; 26:347–55.10.1016/j.neuroimage.2005.02.008 [PubMed: 15907295]

Jones SR, Kerr CE, Wan Q, Pritchett DL, Hämäläinen M, Moore CI. Cued spatial attention drives functionally relevant modulation of the mu rhythm in primary somatosensory cortex. J Neurosci. 2010; 30:13760–5.10.1523/JNEUROSCI.2969-10.2010 [PubMed: 20943916]

Khazipov R, Khalilov I, Tyzio R, Morozova E, Ben-ari Y, Holmes GL. Developmental changes in GABAergic actions and seizure susceptibility in the rat hippocampus. Eur J Neurosci. 2004; 19:590–600.10.1111/j.1460-9568.2003.03152.x [PubMed: 14984409]

Kopell N, Ermentrout GB, Whittington MA, Traub RD. Gamma rhythms and beta rhythms have different synchronization properties. Proc Natl Acad Sci. 2000; 97:1867–72. http://dx.doi.org/10.1073/pnas.97.4.1867. [PubMed: 10677548]

Kuhlman WN. Functional topography of the human mu rhythm. Electroencephalogr Clin Neurophysiol. 1978; 44:83–93. http://dx.doi.org/10.1016/0013-4694(78)90107-4. [PubMed: 74329]

Kybic J, Clerc M, Abboud T, Faugeras O, Keriven R, Papadopoulo T. A common formalism for the integral formulations of the forward EEG problem. IEEE Trans Med Imaging. 2005; 24:12–28. http://dx.doi.org/10.1109/TMI.2004.837363. [PubMed: 15638183]

Lamm C, White LK, McDermott JM, Fox NA. Neural activation underlying cognitive control in the context of neutral and affectively charged pictures in children. Brain Cogn. 2012; 79:181–7. http://dx.doi.org/10.1016/j.bandc.2012.02.013. [PubMed: 22542842]

Lindsley DB. A Longitudinal Study of the Occipital Alpha Rhythm in Normal Children: Frequency and Amplitude Standards. Pedagog Semin J Genet Psychol. 1939; 55:197–213. http://dx.doi.org/10.1080/08856559.1939.10533190.

Manshanden I, De Munck JC, Simon NR, Lopes da Silva FH. Source localization of MEG sleep spindles and the relation to sources of alpha band rhythms. Clin Neurophysiol. 2002; 113:1937–47. http://dx.doi.org/10.1016/S1388-2457(02)00304-8. [PubMed: 12464331]

Marshall PJ, Bar-Haim Y, Fox NA. Development of the EEG from 5 months to 4 years of age. Clin Neurophysiol. 2002; 113:1199–208. http://dx.doi.org/10.1016/S1388-2457(02)00163-3. [PubMed: 12139998]

Marshall PJ, Meltzoff AN. Neural Mirroring Systems: Exploring the EEG Mu Rhythm in Human Infancy. Dev Cog Neurosci. 2011a; 1:110–123. http://dx.doi.org/10.1016/j.dcn.2010.09.001.

Marshall PJ, Young T, Meltzoff AN. Neural correlates of action observation and execution in 14-month-old infants: an event-related EEG desynchronization study. Dev Sci. 2011b; 14:474–80. http://dx.doi.org/10.1111/j.1467-7687.2010.00991.x. [PubMed: 21477187]

Molenberghs P, Cunnington R, Mattingley JB. Brain regions with mirror properties: a meta-analysis of 125 human fMRI studies. Neurosci Biobehav Rev. 2012; 36:341–9. http://dx.doi.org/10.1016/j.neubiorev.2011.07.004. [PubMed: 21782846]

Muthukumaraswamy SD, Johnson BW. Changes in rolandic mu rhythm during observation of a precision grip. Psychophysiol. 2004; 41:152–6. http://dx.doi.org/10.1046/j.1469-8986.2003.00129.x.

Muthukumaraswamy SD, Edden RAE, Jones DK, Swettenham JB, Singh KD. Resting GABA concentration predicts peak gamma frequency and fMRI amplitude in response to visual stimulation in humans. Proc Natl Acad Sci. 2009; 106:2–7.10.1073/pnas.0900728106

Niedermeyer E. Alpha rhythms as physiological and abnormal phenomena. Int J Psychophysiol. 1997; 26:31–49.10.1016/S0167-8760(97)00754-X [PubMed: 9202993]

Nunez PL, Wingeier BM, Silberstein RB. Spatial-temporal structures of human alpha rhythms: theory, microcurrent sources, multiscale measurements, and global binding of local networks. Hum Brain Mapp. 2001; 13:125–64. http://dx.doi.org/10.1002/hbm.1030. [PubMed: 11376500]

Nunez, P.; Srinivasan, R. Electric Fields of the Brain: The Neurophysics of EEG. 2. Oxford;New York: Oxford University Press; 2006.

Nunez, P. Neocortical dynamics and human EEG rhythms. Oxford University Press; 1995.

Nyström P, Ljunghammar T, Rosander K, von Hofsten C. Using mu rhythm desynchronization to measure mirror neuron activity in infants. Dev Sci. 2011; 14:327–35. http://dx.doi.org/10.1111/j.1467-7687.2010.00979.x. [PubMed: 22213903]

Pascual-marqui RD. Reply to Comments Made by R. Grave De Peralta Menendez and S.I. Gozalez Andino. Int J Bioelectromagn. 1999; 1:1–10.

Pascual-Marqui RD. Standardized low-resolution brain electromagnetic tomography (sLORETA): technical details. Methods Find Exp Clin Pharmacol. 2002; 24:5–12. [PubMed: 12575463]

Petsche H, Kaplan S, von Stein A, Filz O. The possible meaning of the upper and lower alpha frequency ranges for cognitive and creative tasks. Int J Psychophysiol. 1997; 26:77–97. http://dx.doi.org/10.1016/S0167-8760(97)00757-5. [PubMed: 9202996]

Pfurtscheller G. Functional topography during sensorimotor activation studied with event-related desynchronization mapping. J Clin Neurophysiol. 1989; 6:75–84. [PubMed: 2915031]

Pfurtscheller G, Aranibar A. Evaluation of event-related desynchronization (ERD) preceding and following voluntary self-paced movement. Electroencephalogr Clin Neurophysiol. 1979; 46:138–46. http://dx.doi.org/10.1016/0013-4694(79)90063-4. [PubMed: 86421]

Pfurtscheller G, Brunner C, Schlögl A, Lopes da Silva FH. Mu rhythm (de)synchronization and EEG single-trial classification of different motor imagery tasks. NeuroImage. 2006; 31:153–9. http://dx.doi.org/10.1016/j.neuroimage.2005.12.003. [PubMed: 16443377]

Pfurtscheller G, Neuper C, Krausz G. Functional dissociation of lower and upper frequency mu rhythms in relation to voluntary limb movement. Clin Neurophysiol. 2000; 111:1873–9. http://dx.doi.org/10.1016/S1388-2457(00)00428-4. [PubMed: 11018505]

Pineda JA, Allison BZ, Vankov A. The effects of self-movement, observation, and imagination on mu rhythms and readiness potentials (RP's): toward a brain-computer interface (BCI). IEEE Trans Rehabil Eng. 2000; 8:219–22. http://dx.doi.org/10.1109/86.847822. [PubMed: 10896193]

Pineda JA. The functional significance of mu rhythms: translating "seeing" and "hearing" into "doing". Brain Res Rev. 2005; 50:57–68. http://dx.doi.org/10.1016/j.brainresrev.2005.04.005. [PubMed: 15925412]

Richards, JE. Attention in the brain and early infancy. In: Johnson, SP., editor. Neoconstructism: The new science of cognitive development. New York: Oxford University Press; 2010. p. 3-31.

Richards, JE. What's inside a baby's head? Structural and functional brain development in infants. International Conference on Infant Studies; Baltimore, MD. 2010;

Ritter P, Moosmann M, Villringer A. Rolandic alpha and beta EEG rhythms' strengths are inversely related to fMRI-BOLD signal in primary somatosensory and motor cortex. Hum Brain Mapp. 2009; 30:1168–87. http://dx.doi.org/10.1002/hbm.20585. [PubMed: 18465747]

Salenius S, Schnitzler A, Salmelin R, Jousmäki V, Hari R. Modulation of human cortical rolandic rhythms during natural sensorimotor tasks. NeuroImage. 1997; 5:221–8. http://dx.doi.org/10.1006/nimg.1997.0261. [PubMed: 9345551]

Salmelin R, Hari R. Characterization of spontaneous MEG rhythms in healthy adults. Electroencephalogr Clin Neurophysiol. 1994a; 91:237–48. [PubMed: 7523073]

Salmelin R, Hari R. Spatiotemporal characteristics of sensorimotor neuromagnetic rhythms related to thumb movement. Neuroscience. 1994b; 60:537–50. http://dx.doi.org/10.1016/0306-4522(94)90263-1. [PubMed: 8072694]

Salmelin R, Hamalainen M, Kajola M, Hari R. Functional Segregation of Movement-Related Rhythmic Activity in the Human Brain. NeuroImage. 1995; 2:237–43. [PubMed: 9343608]

Sanchez CE, Richards JE, Almli CR. Neurodevelopmental MRI brain templates for children from 2 weeks to 4 years of age. Dev Psychobiol. 2011; 54:77–91. http://dx.doi.org/10.1002/dev.20579. [PubMed: 21688258]

Sanchez CE, Richards JE, Almli CR. Age-specific MRI templates for pediatric neuroimaging. Dev Neuropsychol. 2012; 37:379–99. http://dx.doi.org/10.1080/87565641.2012.688900. [PubMed: 22799759]

Smith JR. The Electroencephalogram During Normal Infancy and Childhood: II. The Nature of the Growth of the Alpha Waves Pedagog Semin. J Genet Psychol. 1938a; 53:455–69. http://dx.doi.org/10.1080/08856559.1938.10533821.

Smith JR. The Electroencephalogram During Normal Infancy and Childhood: I. Rhythmic Activities Present in the Neonate and Their Subsequent Development Pedagog Semin. J Genet Psychol. 1938b; 53:431–53. http://dx.doi.org/10.1080/08856559.1938.10533820.

Smith JR. The “Occipital” and “Pre-Central” Alpha Rhythms During the First two Years. J Psychol. 1939; 7:223–6. http://dx.doi.org/10.1080/00223980.1939.9917630.

Smith JR. The Frequency Growth of the Human Alpha Rhythms During Normal Infancy and Childhood. J Psychol. 1941; 11:177–98. http://dx.doi.org/10.1080/00223980.1941.9917028.

Solodkin A, Hlustik P, Chen EE, Small SL. Fine modulation in network activation during motor execution and motor imagery. Cereb Cortex. 2004; 14:1246–55. http://dx.doi.org/10.1093/cercor/bhh086. [PubMed: 15166100]

Southgate V, Johnson MH, El Karoui I, Csibra G. Motor system activation reveals infants’ on-line prediction of others’ goals. Psychol Sci. 2010; 21:355–9. http://dx.doi.org/10.1177/0956797610362058. [PubMed: 20424068]

Southgate V, Johnson MH, Osborne T, Csibra G. Predictive motor activation during action observation in human infants. Biol Lett. 2009; 5:769–72. http://dx.doi.org/10.1098/rsbl.2009.0474. [PubMed: 19675001]

Srinivasan R. Spatial structure of the human alpha rhythm: global correlation in adults and local correlation in children. Clin Neurophysiol. 1999; 110:1351–62. http://dx.doi.org/10.1016/S1388-2457(99)00080-2. [PubMed: 10454270]

Stapel JC, Hunnius S, van Elk M, Bekkering H. Motor activation during observation of unusual versus ordinary actions in infancy. Soc Neurosci. 2010; 5:451–60. http://dx.doi.org/10.1080/17470919.2010.490667. [PubMed: 20602285]

Stone M. Cross-validatory Choice and Assessment of Statistical Predictions. J Royal Stat Soc Series B (Meth). 1974; 36:111–47.

Stroganova TA, Orekhova EV, Posikera IN. EEG alpha rhythm in infants. Clin Neurophysiol. 1999; 110:997–1012. http://dx.doi.org/10.1016/S1388-2457(98)00009-1. [PubMed: 10402087]

Thorpe S, D’Zmura M, Srinivasan R. Lateralization of frequency-specific networks for covert spatial attention to auditory stimuli. Brain Topogr. 2012; 25:39–54.10.1007/s10548-011-0186-x [PubMed: 21630112]

Van Elk M, van Schie HT, Hunnius S, Vesper C, Bekkering H. You’ll never crawl alone: neurophysiological evidence for experience-dependent motor resonance in infancy. NeuroImage. 2008; 43:808–14. http://dx.doi.org/10.1016/j.neuroimage.2008.07.057. [PubMed: 18760368]

Van Overwalle F, Baetens K. Understanding others’ actions and goals by mirror and mentalizing systems: a meta-analysis. NeuroImage. 2009; 48:564–84. http://dx.doi.org/10.1016/j.neuroimage.2009.06.009. [PubMed: 19524046]

Vanhatalo S, Kaila K. Development of neonatal EEG activity: from phenomenology to physiology. Semin Fetal Neonatal Med. 2006; 11:471–8.10.1016/j.siny.2006.07.008 [PubMed: 17018268]

Von Stein A, Sarnthein J. Different frequencies for different scales of cortical integration: from local gamma to long range alpha/theta synchronization. Int J Psychophysiol. 2000; 38:301–13. http://dx.doi.org/10.1016/S0167-8760(00)00172-0. [PubMed: 11102669]

Westfall, P.; Young, S. Wiley Series in Probability and Statistics. Vol. 279. New York: John Wiley and Sons; 1993. Resampling-based multiple testing: Examples and methods for p-value adjustment.

Wolpaw JR, McFarland DJ. Control of a two-dimensional movement signal by a noninvasive brain-computer interface in humans. Proc Natl Acad Sci. 2004; 101:17849–54. http://dx.doi.org/10.1073/pnas.0403504101. [PubMed: 15585584]

Worden MS, Foxe JJ, Wang N, Simpson GV. Anticipatory biasing of visuospatial attention indexed by retinotopically specific alpha-band electroencephalography increases over occipital cortex. J Neurosci. 2000; 20:RC63. [PubMed: 10704517]

Yakovlev, PI.; Lecours, AR. The myelogenetic cycles of regional maturation of the brain. In: Minkowski, A., editor. Regional development of the brain in early life. Oxford: Blackwell; 1967. p. 3-70.

Highlights

1. We compare spectral, topographic, and cortical source structural properties of mu desynchronization and spontaneous alpha band EEG across 12-month, four year, and adult subject groups.
2. Spontaneous upper and lower alpha band peaks increase with age, and central channels contribute more to spontaneous peaks in the upper alpha band in all age groups.
3. Mu desynchronization peaks in the upper alpha band for all groups, and has distributed fronto-parietal cortical representation.

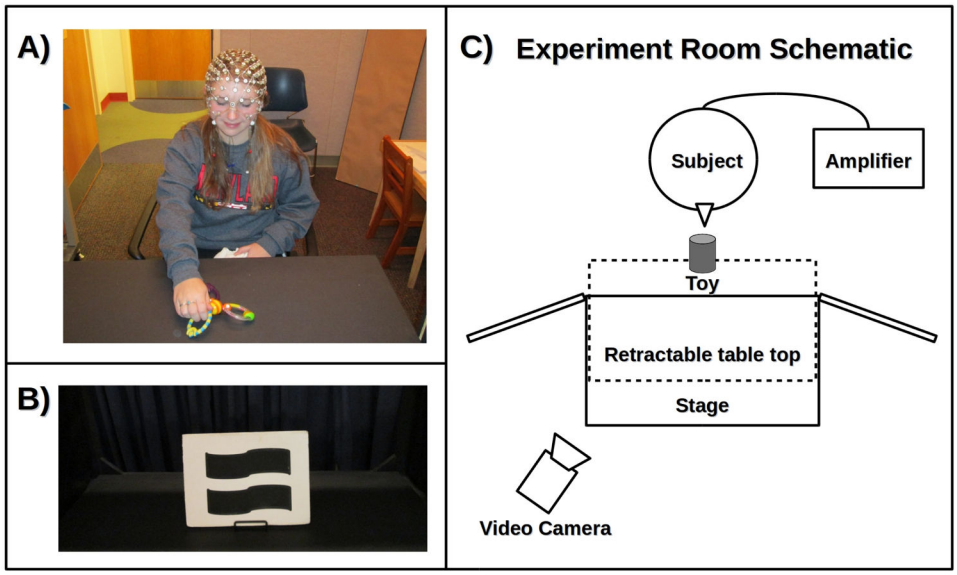

Figure 1.

Experimental setup and participants. Subjects from three age groups corresponding to Adult, 4-year, and 12-month olds completed trials consisting of a three-second baseline interval followed by a grasp execution interval during which the subject reached towards and grasped a toy (A). During the baseline, adult and 4-year subjects viewed a white foam core board with a black shape or pattern (B), whereas 12-month subjects viewed a moving pinwheel. During grasp execution, a toy placed on a retractable table top was pushed toward the subject to within reaching distance (C).

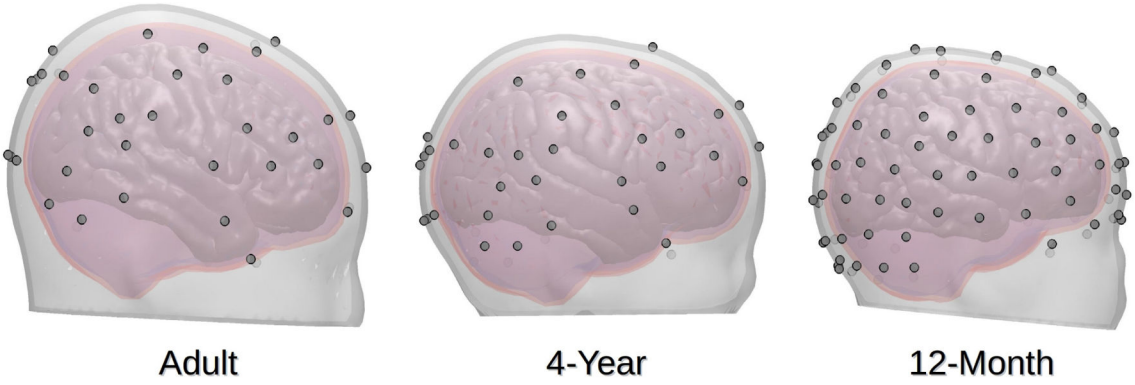

Figure 2.

Age-matched head models with co-registered electrode positions for each subject group, constructed using averaged T1-weighted anatomical templates from the University of South Carolina McCausland Brain Imaging Center Neurodevelopmental MRI Database. Boundary Element Method (BEM) forward models consist of four nested surfaces corresponding to scalp, skull, intracranial space, and gray matter, which were extracted using Freesurfer and MNE software. Forward models were computed using openMEEG, with conductivity values of 0.33, 1.67, 0.0042, and 0.33 for gray matter, intracranial space, skull, and scalp, respectively.

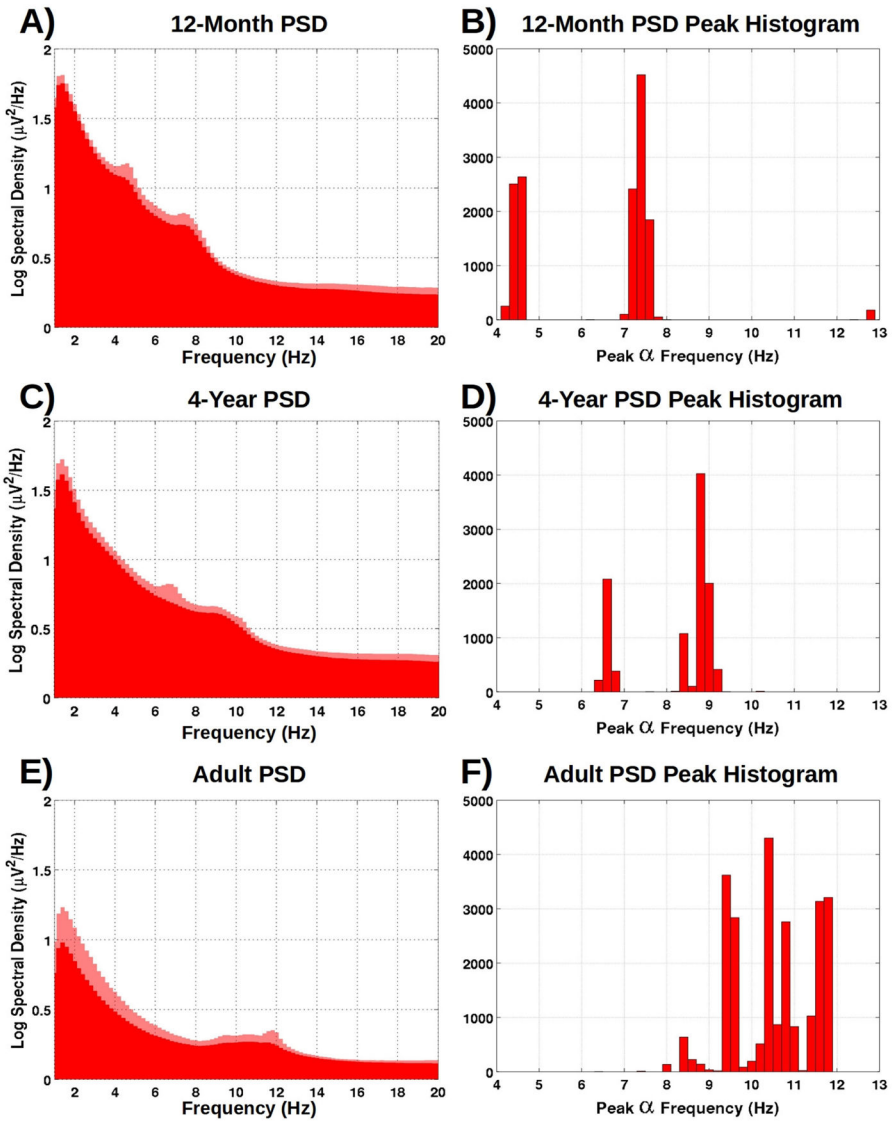

Figure 3.

Log power spectral density by frequency from 1 – 20 Hz for each subject group (A, C, E), along with peak histograms (B, D, F) depicting the variability across bootstrap samples in frequencies at which alpha spectral peaks (between 4 – 13 Hz) were found. Average log PSD across subjects is indicated by red bars, whereas semi-transparent light red bars indicate the 95th percentile of log PSD across bootstrap samples. For 12-month olds, bootstrap sample peaks (B) were tightly clustered in two distinct bands with means of 4.49 and 7.39 Hz corresponding to peaks observed in the mean spectrum (A). 4-year subjects also showed bootstrap peaks (D) which were tightly clustered with mean frequencies of 6.6 and 9.81 Hz corresponding to peaks observed in the mean spectrum (**A**). For adult subjects, the log PSD spectrum (E) didn't show the same clear doubly-peaked structure. Instead, a single broad peak (with mean peak frequency of 10.51) spanning the classic adult alpha range captured 100% of the peak frequency spread observed across bootstrap samples (F).

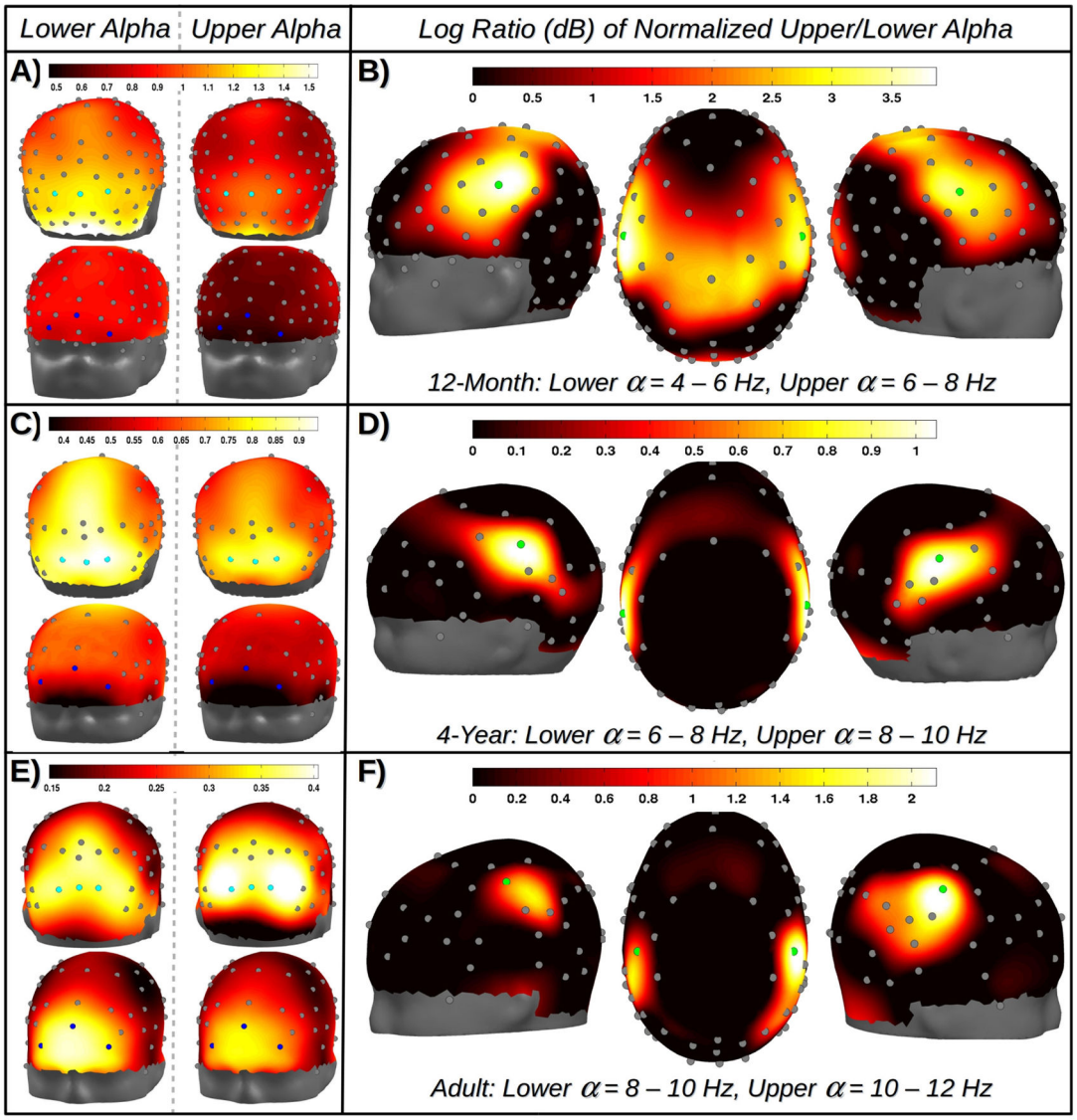

Figure 4.

Upper and lower alpha band topography for each subject group (A, C, E), along with the log ratio of normalized power in the upper/lower bands (B, D, F). Upper and lower alpha topographies (A, C, E) appear superficially similar within each subject group, showing large peaks over occipital electrodes (indicated by cyan), falling off to parietal. Adult subjects show an additional peak at frontal channels (indicated in blue) in both bands as well. The fine structure of topographic differences between these two bands is more readily observable comparing normalized log PSD topographies via log ratio (masked by statistical significance in B, D, F). For all subject groups, bilateral central electrodes show the largest relative contribution to the upper alpha band (C3/C4 electrode locations are indicated by green dots in B, D, E for comparison). For adults and 4-year olds (D, F), foci are tightly clustered about C3/C4, whereas the distribution for 12-month olds (E), while peaking at C3/C4, is more broadly distributed. The distinct bilateral central peaks evident in these maps have long been associated with mu rhythm topography.

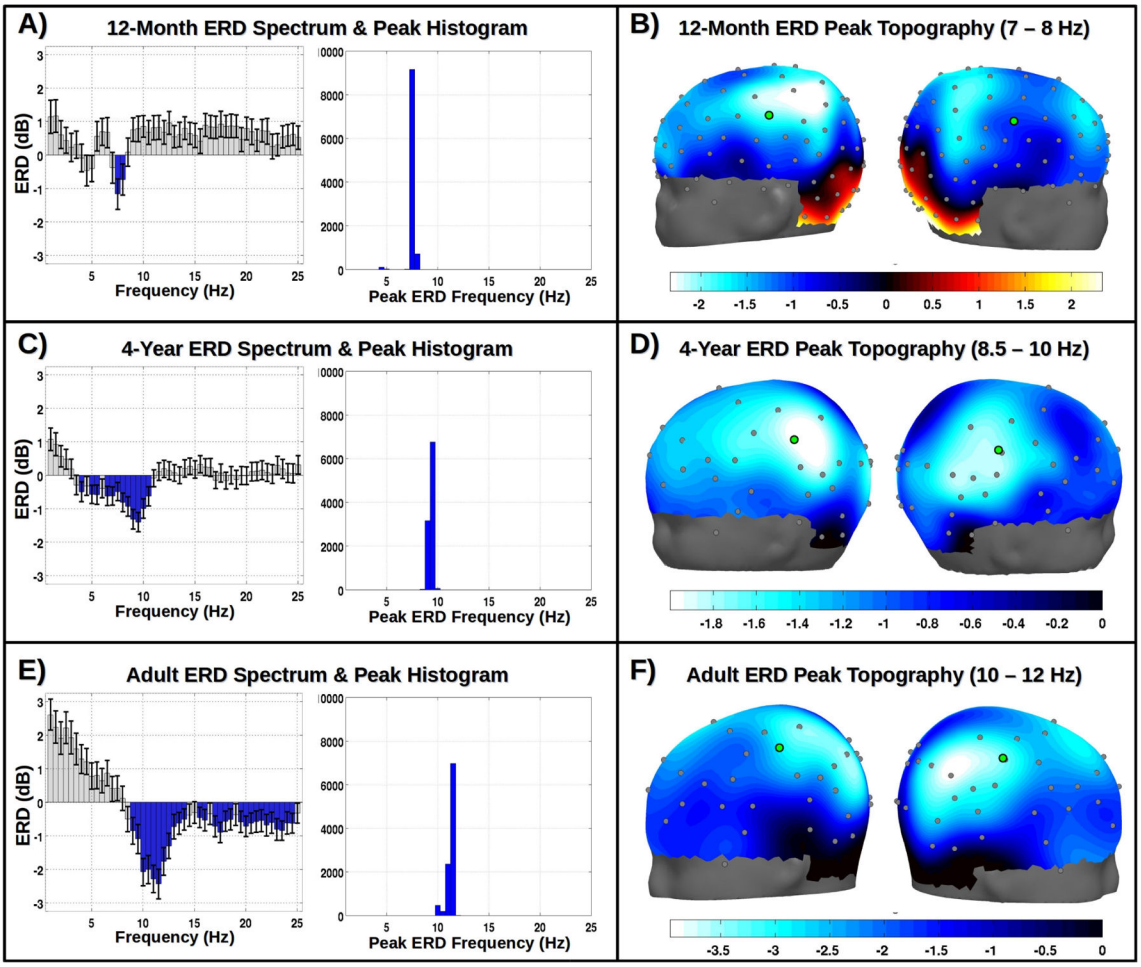

Figure 5.

Channel averaged ERD spectra for each age group (A, C, E, left plot) are indicated by blue bars for frequencies which met significance criterion (and gray bars otherwise), with black error bars indicating 95% bootstrapped confidence intervals. Also shown are histograms (A, C, E, right plot) depicting the variability across bootstrap samples in frequencies at which ERD peaks were found. For 12 month subjects (A) greater than 97.5% of ERD peaks across bootstrap samples were concentrated between 7 – 8 Hz. For 4-year subjects (C) 100% of ERD peaks were contained in the band from 8.5 – 10 Hz. Likewise for adults (E), 100% of ERD peaks were contained in the band from 10 – 12 Hz. For each age group, the band containing the vast majority of ERD peaks across bootstrap samples fell within the upper alpha band identified in figure 3. ERD topography for these designated mu bands of interest is depicted for each age group in B, D, F. Scalp maps show distinct bilateral peaks over central and anterior parietal areas (C3/C4 electrode locations indicated by green dots for comparison), similar to those observed in figure 4.

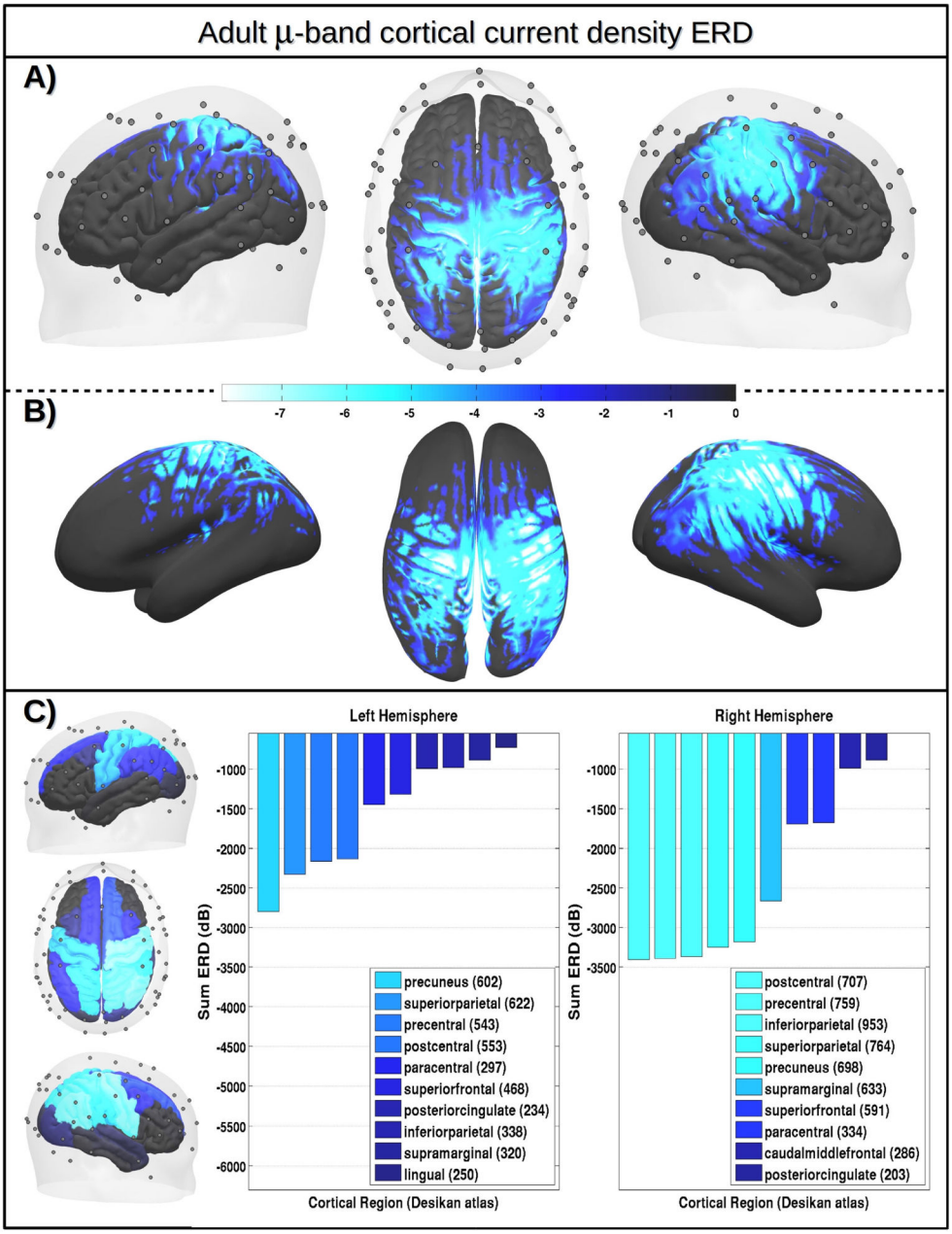

Figure 6.

Cortical mu band desynchronization computed from sLoreta source reconstructions for adult subjects is shown on the reconstructed cortical surface (A), along with the same shown on the inflated surface in order to better visualize ERD in the cortical sulci (B). ERD is shown masked by significance in both maps, such that only data for cortical nodes with ERD significantly less than zero is visualized (adjusted empirical $p<0.05$). A summary of the cortical regions (defined via the Desikan 2006 cortical atlas) which showed the strongest mu band desynchcronization is given in (C), which show ERD summed across all significant nodes within the top ten cortical regions for each cerebral hemisphere, along with representations of these areas on the cortical surface. Mu band ERD is clearly and

consistently greatest in the central and parietal cortices, which account for the majority of the top ranked cortical areas in both hemispheres.

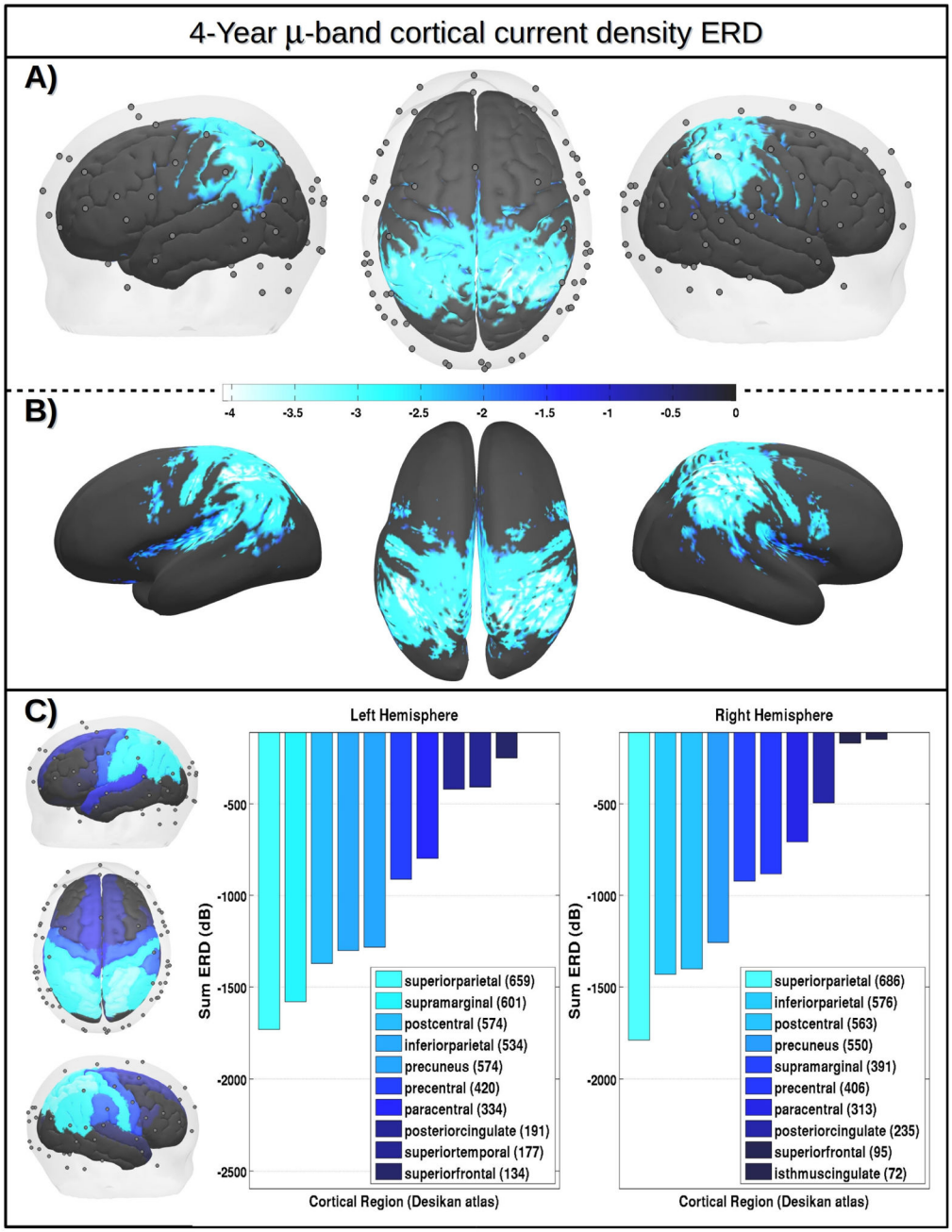

Figure 7.

sLoreta source reconstructions of cortical mu band desynchronization depicted for 4-year subjects similar to figure 6. Similar to the pattern observed for adults, mu band ERD is greatest in the central and parietal cortices, which account for the majority of the top ranked cortical areas in both hemispheres.

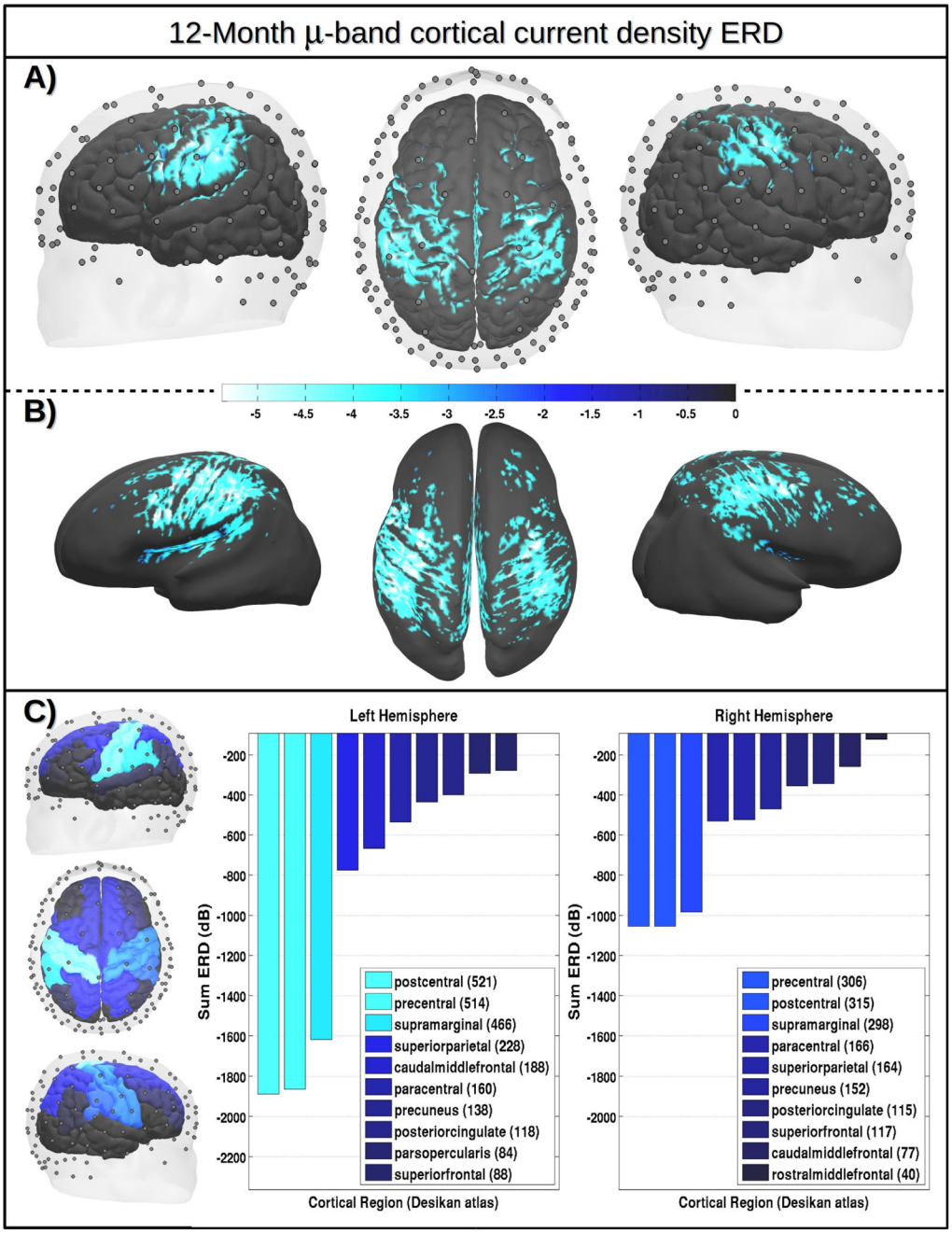

Figure 8.

sLoreta source reconstructions of cortical mu band desynchronization depicted for 12-month subjects similar to figure 6. A similar pattern to that observed for adults and four year olds is evident, with central and parietal cortices accounting for the majority of the top ranked cortical areas in both hemispheres. Specifically, the post-central, pre-central, para-central, and superior frontal areas fall in the top ten for both hemispheres of all subject groups. Similarly, the superior parietal, and supramarginal cortices, as well as the precuneus (all

parietal regions) all fall into the top ten ranked areas for both hemispheres of all subject groups.